Mechanistic Illustrations on Ga-MOF Synthesis Using Spectroscopy and Theory

By

Scholasticah Genchabe Nyamao

Submitted in partial fulfilment of the Requirements

for the Degree of

Master of Science

in

Chemistry

YOUNGSTOWN STATE UNIVERSITY

August 2023

Mechanistic Illustrations on Ga-MOF synthesis using Spectroscopy and Theory

Scholasticah G Nyamao

Signature:

Scholasticah Nyamao, Student Date

Approvals:

Prof. Douglas Genna, Thesis Advisor Date

Prof. Christopher Arntsen, Committee Member Date

Prof. Nina Stourman, Committee Member Date

Salvatore A. Sanders, PhD, Dean, College of Graduate Studies Date

Abstract

Group 13 metals have been used in metal-organic frameworks (MOFs) synthesis with aluminum (Al) and indium (In) producing several of these porous, crystalline, coordination polymers. MOFs have been used in applications like water remediation, gas storage etc. according to their suitability in terms of stability, pore size, chemical composition, among other features. Of the three metals, Gallium is underrepresented with new MOF attempts forming non-MOF/ gel-like outcomes. In this research, we conducted experiments directed towards understanding gallium's preliminary chemical rearrangements, prior to the addition of linker and in the MOF synthesis mixture using *in situ* Raman spectroscopy, density functional theory (DFT) calculations, and synthesis. The initial steps involved experimenting possibilities of a new Ga-MOF through varying synthesis conditions of two known MOFs, Ga-CAU-51 and CAUMOF-11. New MOFs (different metal centers) have been synthesized using this approach. Investigation of Ga^{3+} *solvato* using *in situ* Raman spectroscopic method revealed a consistent Raman band at 345 cm^{-1} in DMF, NMP, and THF: toluene mixed solvent system while Dioxane and THF produced Raman band at 365 cm^{-1}. Solvation of $GaCl_3$ in DMF and NMP was found to be enthalpically favored unlike in dioxane with the possibility to ionize to unsolvated $GaCl_4^-$ or solvated $[GaCl_4 (solv)_2]^-$. Ga-MOF synthesis intermediates that are enthalpically favored led to a node that is known for the formation of anionic Ga-MOF. This anionic form of Ga^{3+} was analyzed in solution and in solid state to assign its unsolvated form to the prominent Raman band at 345 cm^{-1}, that is an intermediate in Ga-MOF synthesis and a starting point for anionic Ga-MOFs.

Acknowledgment

First and foremost, I would like to thank the YSU community, Graduate school, and the Chemistry department and faculty for accepting and granting me the admission and Graduate assistantship opportunity for the Master's in Chemistry program. Also, I register my sincere gratitude to the professors that I have worked with both as a student and a Teaching Assistant, Dr. Genna, Dr. Stourman, Dr. Simeonson, Dr. Norris, Dr. Leskiw, Dr. Arntsen, and Dr.Hunter who have put an indelible impact in my career life. I will forever be grateful for their dedication and the passion they demonstrated.

Additionally, my deepest appreciation goes to Dr. Douglas Genna in both his role in the department as the Director and as my supervisor. It's Doug's kind gestures, empathy, prompt communication, and hands-on guidance that have propelled me to this level. You created a safe space where I could pour-out my concerns on aspects of coursework, Research, career and parenting. The inspiring nuggets will walk me far and beyond. Thank you for shaping and reenergizing, boosting my confidence, and cultivating a culture of reading pertinent to the completion of my research work.

I appreciate you for allowing me to work in the Genna Lab where my interest in organic research was awaken. It's here that I met passionate researchers and versatile colleagues; Jennifer Moore, Vincent DelFratte, Nicholas Fromel, and Nicholas Scarl. Amidst your busy schedules, you made time for me to assess my progress and ensure that I am on the right path. The chit chat moments prior to our weekly meetings that brought about plenty of laughter were therapeutic!

I would like to highlight one special person whom I will forever hold dear in my life, my son, Esteban Mich. Son, you have been the most amazing child anyone will wish for. Thank you for being understanding and giving me an easy time during this period when I had to do what I had to do, for us. To my family, you have been there for me since the start. I appreciate your prayers, words of encouragement, and positive thoughts. I won't forget to thank my colleagues Chemistry class of 2023, this journey has not been a roller coaster but you all made it beautiful and worthwhile. Best wishes to you in your future endeavors.

Table of Contents

List of Figures

CHAPTER I: INTRODUCTION

1.1 MOFs

Metal-organic frameworks (MOFs) are crystalline, porous coordination polymers that are constituted of organic and inorganic building blocks (Figure 1). These materials can be connected along two or all three Cartesian coordinate axes; this makes MOFs valuable targets for application.[1] MOFs have been used for several applications, including gas storage, nano-medicine, water purification, environmental carbon capture, sensing and others.[2,3,4,5] The applicability of the different MOFs is dependent on their thermal and chemical properties which vary from one type to another.[6]

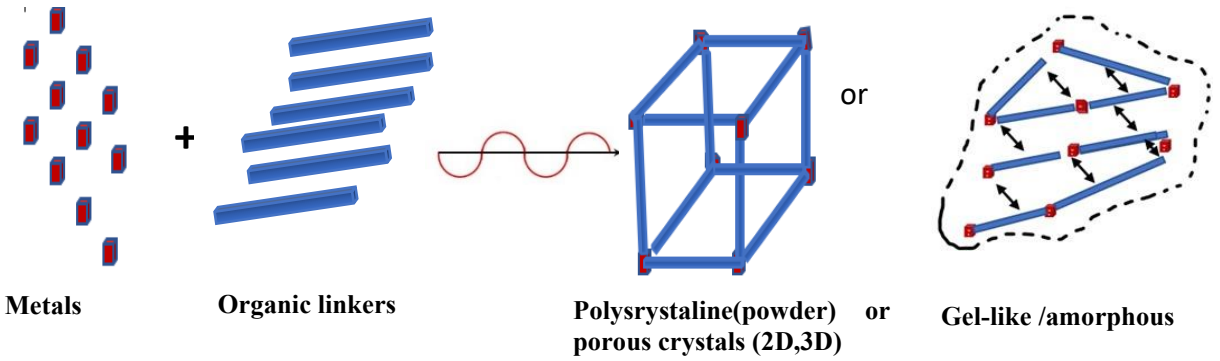

Figure 1: MOFs synthesis process.

Metal ions and organic linkers interact under given temperature conditions and/or other additives such as solvent and modulators. Sometimes the MOF doesn't form despite the conditions as in the case of Ga-MOF diversification. Synthesizing MOFs with desirable attributes of porosity, stability, and phase purity remains an uphill task. Since these are very important features required for their varied applications, they can be realized through the optimization of suitable synthetic conditions. One-way large pore size is a preferred quality as it relates directly to uptake capacity of a MOF and it's achieved by increasing the length of the linkers used in synthesis. However, in some cases, the resulting MOFs were found to be less porous and ultimately denser than predicted. Only in a few cases has the structural outcome of a MOF has been predicted and even tuned appropriately for particular uses of the resulting MOF.[7]

Solvothermal technique used in MOF synthesis may cause the channels and cages of freshly grown MOF components to be occupied by solvents deployed as reaction media in elevated temperatures. This clogged material can be evacuated through MOF activation procedures to ensure that the final crystalline product is sufficiently porous for further exploration of its properties.[8] Ultimately, MOFs undergo extensive characterization post-synthesis, to ascertain their structural features. Single-crystal X-ray diffraction (SXRD) is the standard for structural elucidation while powder X-ray diffraction (PXRD) will give a confirmation of the identity of the bulk material.

Numerous MOF structures (more than 70,000) have been synthesized from different metal centers.[9] Comprehension of the factors that determine the type and quality of already established MOFs is a pathway to achieve fast and accurate synthesis of new materials. However, there is still much to explore on the chemical transformations during MOF growth processes that are yet to be exhausted in order to contribute to the library of information in this line of synthesis. Gallium-derived MOFs have been difficult to synthesize and only a few select examples are known in the literature.[6]

1.2 Group 13 MOFs

Group 13 MOFs have been studied extensively whereby the majority of MOF structures have been built with *N*-donor, carboxylate, phosphonate, or sulfonate linkers. A lot of information on their formation and tuning has been explored as well as their suitability in numerous applications such as toxic gas capture and catalysis.[10] Due to the availability of Al salts, a lot of MOFs have been synthesized using Al^{3+} as the metal center. Additionally, Al is relatively affordable and abundant and this makes it an appealing source for the production of MOFs.

Indium-derived MOFs are predominantly comprised of carboxylate ligands. In-MOFs have been deployed for gas adsorption, separation, as well as fluorescence detection.[10,11] The Genna Lab has extensively studied In-MOF formation. In one of their papers,[12] they successfully synthesized six different In-MOFs including the previously reported ATF-1, YCM-22 (YCM= Youngstown Crystalline Material), anionic YCM-21, and infinite chain YCM-23. They are built on anionic, dianionic, anaionic and neutral nodes respectively. All these MOFs were derived from thiophene-2,5-dicarboxylic acid (H_2TDC) alone as the linker, Figure 2.

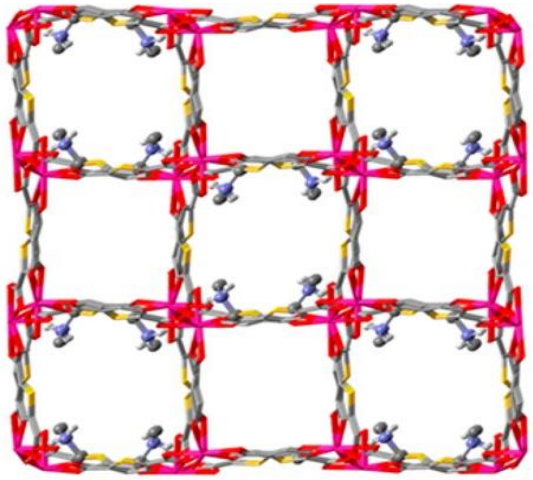

ATF-1

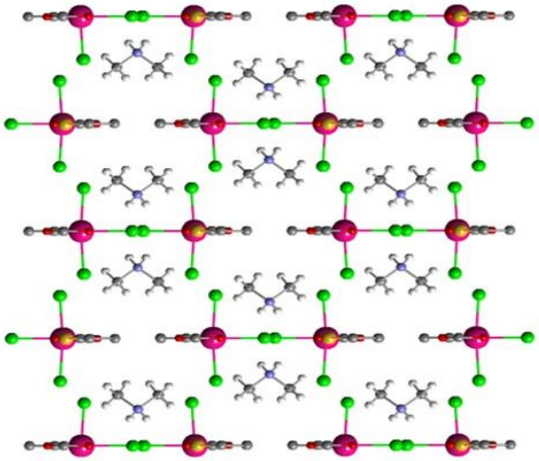

YCM-22

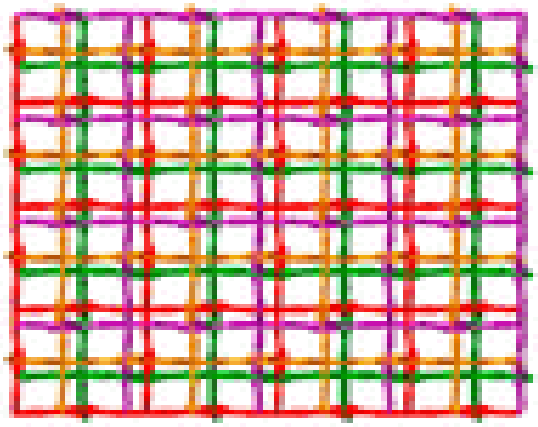

YCM -21-Z

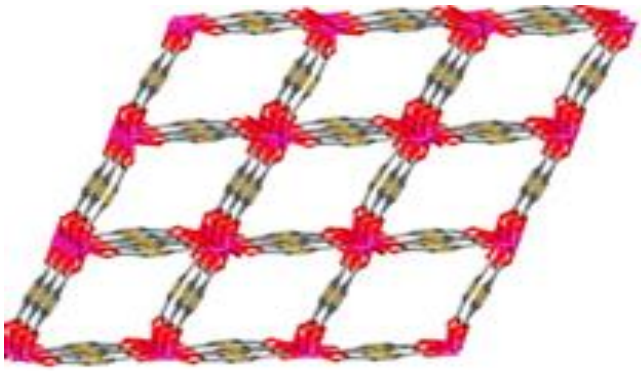

YCM-23

Cryst. Growth Des. 2016, 16, 3, 1550–1558

Figure 2: Varieties of In^{3+} MOFs obtained from H_2TDC as a linker.

The additives subscribed provided different chemical medium in terms of PH and the available ions, which stirred the reaction to different outcomes as shown in Figure. 3. This was spearheaded by the understanding of the different nodes that In^{3+} can form in varying synthesis conditions as influenced by modulators such as acidic or basic conditions. The node is an anchoring repeating unit unto which groups attach to form a geometrically and chemically stable MOF. It derives overall charge from the arithmetic involving total ligands attached to the metal center and mostly this is the MOF charge. Genna and group explicitly described the suitable synthesis conditions (anion type and concentration, organic linker, and important additives), stability of the MOF, and structural morphology.

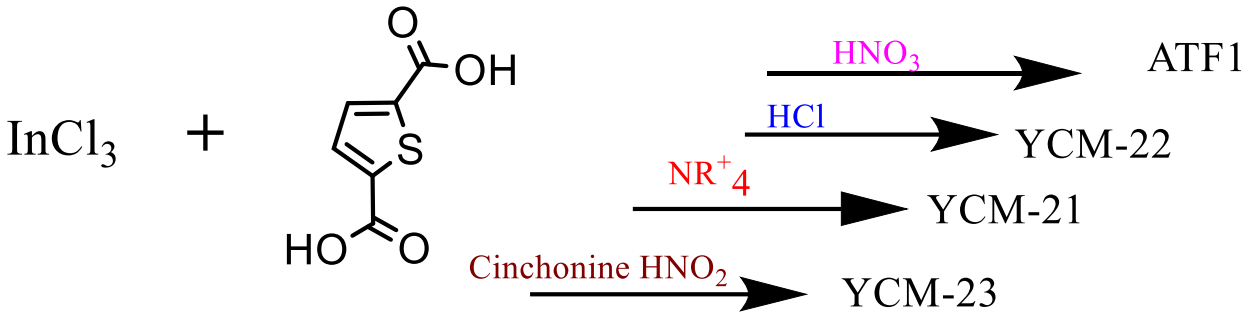

Figure 3: Diversity of indium MOFs from H_2TDC linker with different additives.

The coordination chemistry for In secondary building units (SBU) was established to be monomeric, infinite chain, or trimeric (Figure 4 a, b, and c respectively) which indicates different MOF possibilities.[12]

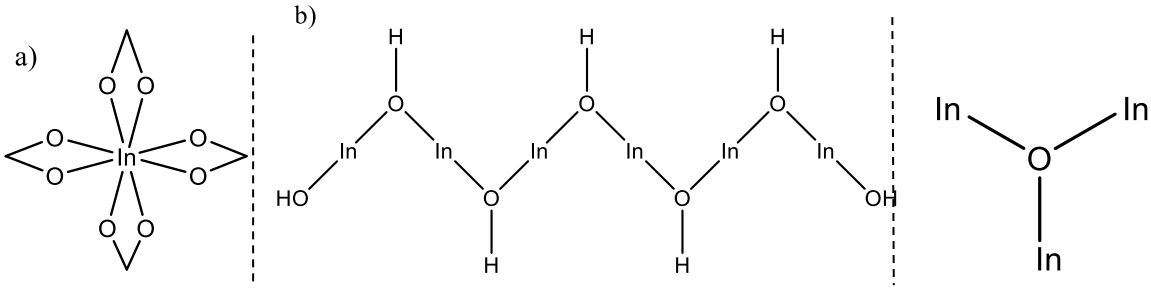

Figure 4: Coordination of In-SBUs. a) monomer, b) infinite chain c) trimer

In a study on the role of solvent in MOF synthesis, Genna *et al.*[1] carried out experimental and computational analysis of the structure of $InCl_3$ in different organic solvents. This involved energy calculations of the coordination possibilities of In^{3+} in organic solvents combined with time-dependent Raman spectroscopy that monitored the reaction to determine the enthalpically favored conformation and ultimately carry out the MOF synthesis.[1] A similar concept for the study of Ga to understand its potential in this noble synthesis was recommended.

In exploring their properties, Al-MOFs are classified as having remarkable sorption properties and stability.[13] A study by Shengfu Ji *et al.* has for example demonstrated the catalytic property of MIL-53 in the Friedel-Craft acylation reaction to synthesize 3-acylindole which is a precursor molecule in anti-tumor drug synthesis.[14] Another MOF synthesized from Al^{3+} is MIL-68, which according to the research by Liao *et al* can be used in the capture of acetic acid from the atmosphere.[15] Other well-studied aluminum MOFs include the Materials Institute Lavoisier (Al-MIL) and Christian-Albrechts-University (Al-CAU) types to mention a few.[16]

Most of these studied Al-MOFs are neutral. However, Fischer has recently made advancements in the synthesis of anionic Al-MOFs by pioneering formation of a crystalline Al-Td-MOF-1 with permanent porosity and good ion conductivity. Firstly, they synthesized an amorphous aluminate framework from 1,4-dihydroxybenzene and lithium aluminum hydride followed by a solvothermal process under alkaline conditions to arrive at the MOF.[17] Anionic MOFs are deemed to have potential for a wide range of applications including but not limited to drug delivery and ionic conductivity due to the ability to load both metallic and organic cations.[18]

Group-13 MOFs have been identified to form a characteristic infinite chain of octahedral units linked by ligands such as terephthalate from terephthalic acid.[19,20,21] Due to their chemical similarity Ga^{3+} is hypothesized to form similar SBUs to In^{3+} and Al^{3+}. However, synthesizing Ga-MOFs under comparable conditions to In-MOFs has been difficult. For example, Genna has shown that 6 different MOFs comprised of In^{3+} and H_2TDC can be synthesized, but only a single Ga-MOF (CAU-51), reported by Stock, has been synthesized from the same H_2TDC linker, shown in Figure. 5a.[13]

When compared with Al and In MOFs, Ga has not received sufficient attention in group 13 MOFs.[6] Anecdotally, attempts to synthesize Ga-MOFs often result in gel-like or amorphous products that are challenging to characterize. The reason for this discrepancy amongst the group 13 metals has yet to be elucidated. We hypothesize that if the fundamental steps of Ga-MOFs can be revealed, then crystalline materials could be synthesized, allowing for robust Ga-MOF synthesis. This is important since to date the applications of Ga-MOFs is not understood, simply because there haven't been enough Ga-MOFs available to study.

1.3 Synthesis of MOFs

Several parameters affect the coordination tendencies of metal centers and organic ligands which have a major role in the quality of outcomes and reflect directly in the structure of MOFs. The reaction time, solvents, and reaction temperatures are the major aspects that come into play while preparing MOFs.[22,23,24] DMF is the most commonly used solvent where it is applied as a mono-solvent or in a mixed system unto which another solvent is added to it.

Particularly, DMF has several roles in synthesizing MOFs, including solubilizing the components in the reaction and serving as a chemical reagent attributable to its decomposition into dimethyl amine (Me_2NH) and carbon monoxide (CO) or formate ($HCOO^-$). This is increasingly important

in the creation of anionic MOFs which need charge-balancing cations, which are often in the form of $[Me_2NH_2]^+$. The formic acid or formate has been classified as an *in situ* modulator during the production of several MOFs.[25] Moreover, DMF has demonstrated the ability to act as a ligand for several metals deployed in MOF synthesis.[26] This shows the sophisticated role that DMF plays and presents a challenge to explore the potential of other solvents beyond just the solubilization of starting materials.

Application of solvothermal synthesis significantly promotes the crystallization progression attributable to improved solubility of raw materials and hence high-quality crystals created.[22] Stock and co-workers describe it to have the advantages of being simple and affordable besides allowing for utilization of non-readily soluble starting material. This group also demonstrated the technique's additional provisions such as change of starting chemical material and synthesis conditions to suit the targeted outcomes.[6] Several experiments in this system have demonstrated the use of modulators and other additives such as water (H_2O), nitric acid (HNO_3), and tetraethylammonium chloride ($Et_4N^+Cl^-$) in various temperature and pressure conditions during the self-assembly of MOFs. Solvothermal synthesis also accommodates higher pressure, beyond 1 atm, and higher reaction temperatures, more than 100 °C for closed systems.[27]

There is a growing area of research that focusses on the use of mechanochemical approach in the synthesis of coordination complexes including MOFs and polymers. This synthetic approach, offers another option to the traditional solution-based approach for synthesizing MOFs.[28] The approach is increasingly convenient, quick and it avoids or minimizes the quantity of solvent utilized. Nonetheless, there is little knowledge about the extent of this method and the aspect that regulate the reactivity and characteristics of the materials prepared through this approach.

In a study that utilized this technique, the researchers described a solvent-free mechanochemical synthesis process for microporous MOF $[Cu(INA)_2]$ (INA = isonicotinic acid).[29] The product revealed a robust three dimensional structure obtained through crushing isonicotinic acid coupled with copper acetate without applying any heat. The illustrated potential of this synthesis methods warrants further study to ascertain its efficiency in wide range MOF synthesis.[29]

MOF studies that target the understanding of step-by-step growth and identifying points of intervention, have utilized *in situ* microscopy to monitor the process. *In situ* atomic force microscopy (AFM) has demonstrated that the copper MOF, HKUST-1, grows by the step-wise addition of monomeric units of both linker and metal cation.[30] Using UiO-66, growth was documented due to the addition of building units[31] and evidence has emerged to support the involvement of an amorphous-to-crystalline reorganization.[32] Other studies indicate that MOF synthesis might involve solid-to-solid reorganization to achieve a porous crystalline material.[27]

Valuable insights on the formation of MOFs have been obtained through other spectroscopic methods including small angle X-ray scattering (SAXS) and *in situ* X-ray diffractometry XRD as well as nuclear magnetic resonance (NMR), Raman spectroscopy, and infrared spectroscopy (IR).[33,34,35,36] Gascon *et al.* deployed *in situ* energy dispersive X-ray diffraction (EDXRD) and SAXS to illustrate the use of amino-functionalized terephthalic acid in the synthesis where water promoted the formation of the thermodynamically preferred NH_2-MIL-53 (AI) product instead of the kinetic NH_2-MIL-101 (AI) product that was formed in DMF.[37] In another exploration, Cravillon *et al*.[38] showed the formation of 1 nm cluster species using time-resolved SAXS/WAXS as a prenucleation cluster before the formation of ZIF-8. Prenucleation building units (PNBUs) that form during solvation serve as precursor species for secondary building units (SBUs) as

described by Taulelle *et al* in their work involving synthesis of $AlPO_4CJ2$ using *in situ* liquid NMR investigation.[39]

Distaso *et al*. [35] studied the formation of MIL-53 (Al) in DMF using simultaneous Fourier-transform infrared (FTIR) and Raman spectroscopy. The two spectroscopic techniques have the advantage of showing the progression the reactions with the different intermediates generated in the process of MOF synthesis while they occur.[39] The researchers collected turbidity *in situ* within a custom-developed solvothermal reactor. MOF synthesis, from starting materials (linker and aluminum metal center) in suitable conditions were followed using time-resolved Raman and FTIR. The formation of PNBUs, their assembly to MIL-53, DMF decomposition to formic acid and dimethylammonium and ultimate assembly of the MOF crystals were observed.[35,40,41,42] Raman peaks for individual solvated starting materials were compared with those arising from the MOF synthesis phases which confirmed the presence of MOF intermediates described in the literature. Further affirmation of the PNBU phase, was the absence of MOF particles, after a significant reduction from the starting concentration of the linker as observed on the spectra. The rate for each step was calculated from the activation energies requirement and the rate-determining step was determined to be the formation of the crystalline MOF from the PNBUs.[31,33]

In their *in situ* MOF explorations Distaso *et al*.[40] further examined the role of DMF in the solvothermal synthesis of MIL-53 (Al) where dry DMF vs water-DMF mixtures were investigated using *in situ* Raman spectroscopy. The effect of this solvent system on the formation of intermediate PNBU species consisting of linker molecules and metal atoms was analyzed and the findings showed that PNBU concentration was affected by the solvent polarity and in return yielded different quality MOF crystals with the best particles being in dry DMF conditions. They attributed this observation to the role of linker availability/concentration in the reaction mixture whereby at low linker solubility, the PNBU phase was bypassed post-linker deprotonation in the MOF synthesis process.[40,41] Some phases were shown to be temperature dependent while others were not. The effect of linker solubility and concentration of PNBU in the synthesis MIL-53(Al) were elaborated for reference on similar MOF syntheses.[40] Their previous work on the characterization of the same MOF played a role in discerning the phases involved in the synthesis.

Informed by these works, we took a similar route to illustrate mechanistically the Ga-MOF behavior while putting into perspective the solvation of the inorganic component in different organic solvents and DFT calculations on enthalpy, which were in agreement with *in situ* Raman analysis in same solvent systems and following the actual Ga-MOF synthesis using *in situ* Raman for comparison on the findings. This shows the usefulness of vibrational spectroscopy and XRD when utilized for real-time monitoring of MOF growth processes for better insights into the chemical processes.

To date, there is only one known anionic Ga-MOF Figure 5b.[43] It has been synthesized from a tri-topic organic linker, benzene-1,3,5-tricarboxylic acid (H_3BTC) also known as trimesic acid.[44] In the pursuit of expanding the library of anionic Ga-MOFs, we began an experimental and computational investigation into the behavior of Ga^{3+} in solution. The question that we seek to answer is why Ga- MOFs fail to form when Al and In MOFs form readily in similar synthesis conditions.

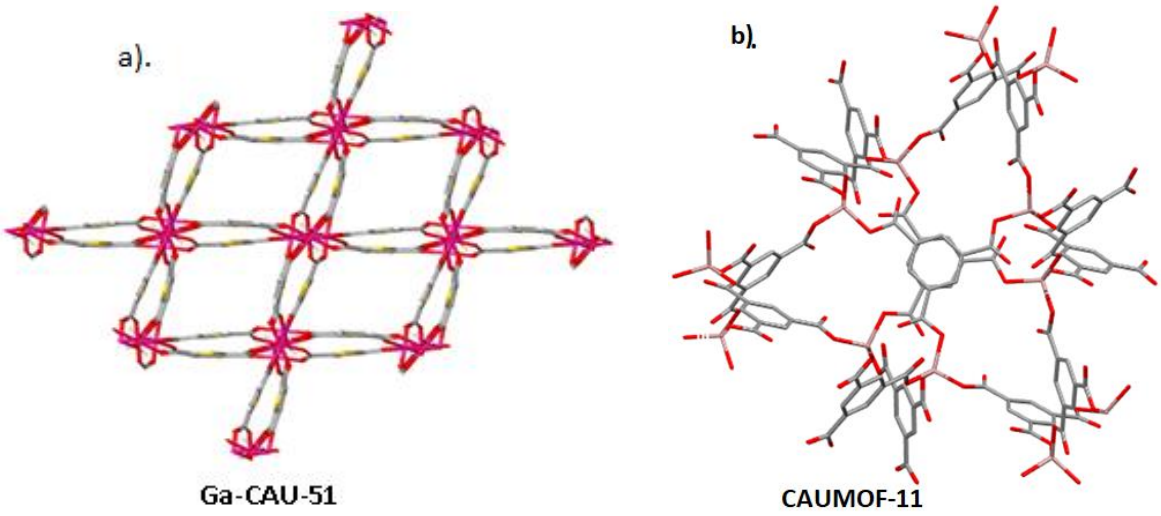

Figure 5: a) Ga- CAU-51 from H_2TDC linker. b) CAUMOF-11 from the trimesic acid linker

Solvation of MOF raw material in the initial step of the synthesis is essential for the progress of the self-assembly process. The benefits of understanding the mechanisms of MOF self-assembly include reduction of synthesis time and wastage of material due to the trial and error that is often the case in the pursuit of attaining new MOFs. Any significant strides made towards the realization of how MOFs form would help even in the synthesis from Ga^{3+}. In this research, we implemented *in situ* Raman spectroscopy using a custom-built Raman oven Figure 6, to monitor the solvation process of the starting materials in different organic solvents and the actual MOF mixture.

Figure 6: Raman probe fitted in dark box.

1.4 Research Problem

MOFs continue to be studied due to their endless potential for applications, be it drug delivery, gas storage, CO_2 capture, and water purification, among other uses.[40] Despite wide acknowledgment in research regarding the varied applications of MOFs, their formations are not fully comprehended. For instance, in solution, the organic and inorganic elements undergo self-assembly to critical masses capable of nucleation. All the while, the inorganic molecular building units (MBUs) need to be formed from simple inorganic initial materials *in situ*. Furthermore, most metals have been found to yield several SBUs such as indium alongside the group 13 metals that are able to access three or more varied SBU/MBU combinations: a cationic $[In_3(O_2CR)_6(H_2O)_3]^+$, anionic $[In(O_2CR)_4]^-$, and a neutral $[In(\mu\text{-}O_2CR)_2(\mu\text{-}OH]_\infty$ infinite chain.[1]

Attributable to the multifaceted nature of MOF synthesis, there is a need for extensive exploration to comprehend their formation in post- and pre-nucleation. A general evaluation of the group 13 MOFs reveals that the majority have been synthesized from Al^{3+} and In^{3+}. Particularly, the Genna Lab has synthesized and is still exploring the synthesis of different MOFs from In^{3+}. There is little knowledge regarding Ga-MOFs; the Genna Lab has been able to synthesize only one Ga-MOF (Ga-CAU-51), Figure 5a. Ga-MOFs could be cheaper in production compared to In-MOFs considering the cost of raw materials, besides the possibility of offering something in the MOF genre that we do not currently know of. Therefore, comprehending the synthesis of Ga-MOFs is an increasingly vital aspect due to its many potential uses. This study will examine the formation of Ga-MOFs, and the behavior of Ga^{3+} as a metal center in solution, both experimentally and computationally.

1.5 Objectives

This exploration focused on examining the possibilities of a new Ga-MOF through varying synthesis conditions of temperature, linker, additives and solvent used in the synthesis of two known MOFs, CAU-51 and CAUMOF-11. We hypothesized the possibility of generating new MOFs by changing the reaction parameters of organic linkers and solvent, synthesis temperatures and pressure. The solution phase structure of Ga^{3+} was investigated using *in situ* Raman spectroscopy in addition to computations to determine the complexes formed in the reaction mixture during MOF synthesis.

Studies have demonstrated the significance of understanding the chemical changes with In^{3+} as starting material in solution, and we hypothesize that this should be similar for Ga^{3+}in solution. However, since little is known about Ga-MOFs, the directions one can take are nearly limitless in terms of choice of a linker, modulator, temperature, and other parameters. Just as in In-MOF synthesis, understanding the structure of Ga^{3+} in solution is important. The focus of this study involves identifying the changes that occurs to the starting material, $GaCl_3$ in solution as an initial intervention for a well-structured MOF outcome. Therefore, the initial work concentrated on using DFT calculations where bonding energies are calculated by generating coordinates of the built molecular compounds with the correct bonding topology and charge, followed by optimizing coordinates in Q-chem to generate enthalpies that can be compared across an array of structures.

This work involves the *in situ* analysis of the intermediates formed from the starting materials in the synthesis mixture in relation to the possible starting point in the anionic Ga-MOF synthesis. The identified intermediate is compared to the products of Ga^{3+} solvation to ascertain the actual intermediate required for successful Ga-MOF outcome. The organic linkers in this work are thiophene-dicarboxylic acid (H_2TDC), trimesic acid, isophthalic acid, (meso-tetra

carboxyphenylporphine (TCPP) and terephthalic acid, Figure 7, in the presence of tetraethylammonium chloride ($Et_4N^+Cl^-$) in NMP, DMF, THF, dioxane and toluene solvent systems. Other additives like water and HNO_3 were incorporated. We also carried out *in situ* Raman analysis of $GaCl_3$ and $Ga(NO_3)_3$ in solution across the different solvents at different temperature conditions, room temperature and 65 °C, in addition to MOF synthesis process analyses. We hypothesized that by identifying the stepwise chemical transformations in the reaction mixture, we would be able to identify a working procedure for the synthesis of new crystalline Gallium material.

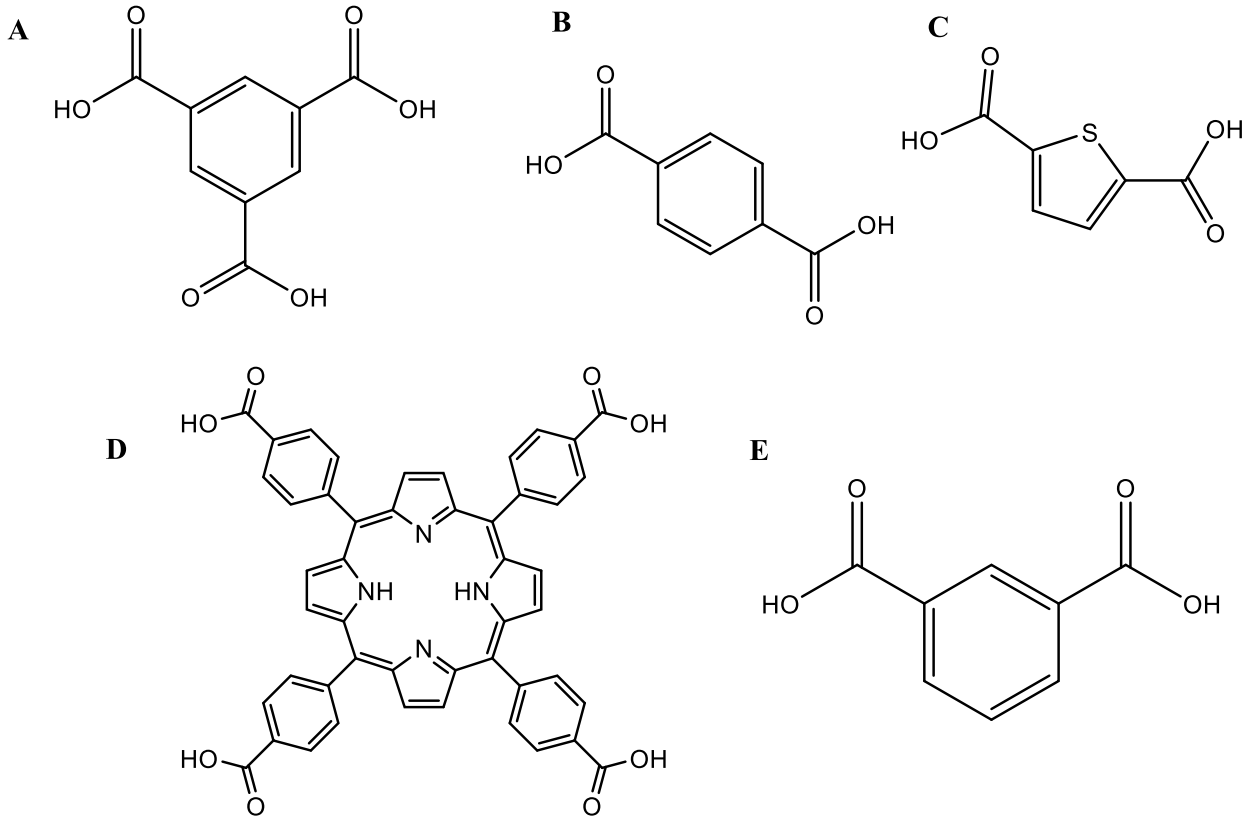

Figure 7: Organic linkers, A) trimesic acid B) Terephthalic acid C) 2,5-thiophenedicarboxylic acid D) meso-tetra carboxyphenyl porphin and E) Isophthalic acid.

CHAPTER II: EXPERIMENTAL SECTION

2.1 Materials and Methods

2.1.1 Reagents and Instrumentation

$GaCl_3$, Granular 99.999%-Ga, and $Ga(NO_3)_3.H_2O$ 99.9% -Sc were purchased from Strem Chemicals Incorporated), 2,5-H_2TDC >98% titration, Trimesic Acid 95%, $Et_4N^+Cl^-$ ⩾98%, $Pt_4N^+Cl^-$, DMF and 1,4-Dioxane were purchased from Sigma Aldrich. THF, HNO_3, DCM and Toluene were purchased from Fisher Chemicals. NMP was purchased from Bioplus Chemicals, and Deionized H_2O from the tap was used.

2.1.2 Incubation synthesis

Syntheses in the ovens were performed in custom-made steel autoclaves equipped with Teflon vials that have capacity to hold 10 mL with a total volume of 12 mL, for high temperature and pressure experiments. Other syntheses were carried out in 20 mL glass vials sealed with Teflon lining.

2.1.3 Computational simulations.

DFT calculations were done using, ωB97X-D functional, and 6-316G* basis set, and an implicit solvent model. Molecular structure geometries, built in Spartan with the correct bonding and charge, are optimized in Q-chem and then the generated enthalpies of optimized structures were used to perform Hess Law calculations.

2.1.4 X-ray Powder Diffraction

Powder XRD patterns of small samples were collected on a Bruker AXS X8 Prospector CCD single crystal diffractometer using the "pilot" plugin for the collection of multi-crystalline XRD patterns. The instrument is equipped with a copper IμS microsource with a laterally graded multilayer (Goebel) mirror for monochromatization (λ = 1.54178 Å, beam size 0.1-0.2 mm) and an ApexII CCD area detector. Powder samples were thoroughly ground to assure a representative number of crystallites to be present in the X-ray beam. Powder samples were mixed with small amounts of mineral oil and mounted onto a 0.4 mm diameter Mitegen micromesh mount for data collection. Samples were centered in the beam using the instrument's mounting microscope video camera. Data were collected in an emulated theta-2theta setup using the Apex2 software package of Bruker AXS. The sample mount was aligned horizontally (χ= 0°) and theta angles were set to eight different angles between 12 and 96° to cover a range equivalent to a 0 to 110° range of a powder X-ray diffractometer operated in Debye Scherrer mode (omega angles of each run were set to half the theta values). Samples were rotated around the mount's spindle axis during measurement (360 rotation around phi), typical exposure times were 30 seconds per frame collected. The eight individual patterns taken were corrected for the unequal sample to detector surface distance ("unwarped") and were combined into one continuous pattern using the "pilot plugin" software embedded in the Apex2 software package. Data were integrated over 2 θ, converted in powder XRD patterns in Bruker "raw" format and further processed with standard powder XRD software packages.

2.1.5 *In situ* Raman

Raman spectroscopy was conducted using a custom-built Raman oven fitted with a 785 nm fiberoptic probe from Kaiser Optical Systems. The data collected in text file format was converted to a CSV file for analysis using MATLAB.

2.1.6 Solid state Raman

Dried powder samples were put under fiberoptic probe fitted with lens for single scans.

2.1.7 Drying samples

Samples were washed with respective solvent and separated from solvent post centrifugation. They were then dried in the vacuum pump overnight at room temperature.

2.2 Experimental procedures

2.2.1 Synthesis of Ga-MOF

We started by reproducing the known MOF, Ga-CAU-51 and CAUMOF-11, under the original synthesis conditions followed by other alterations of the starting materials in attempt to derive a new MOF. The synthesis temperature and pressure conditions were maintained except for when we ran the *in situ* Raman where glass vial was used in place of the autoclave set and the sustained temperature for Raman could not go beyond 135 ^{o}C.

2.2.1.1 Ga-CAU-51

a) Using H_2TDC

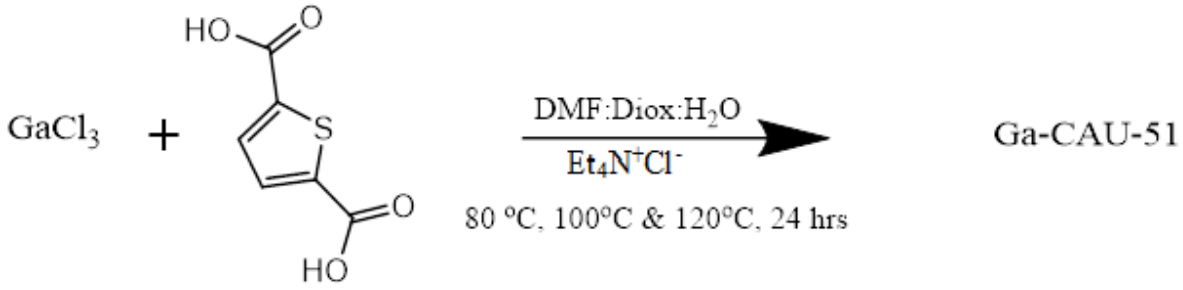

Figure 8: CAU-51 synthesis using H_2TDC linker.

Ga-CAU-51 was synthesized according to the original procedure described by Stock.[13] Into 3 vials 20 mL each, $GaCl_3$ (0.232 g, 0.001mols, 1 equiv) and $Et_4N^+Cl^-$ (0.186 g, 0.001mols, 1 equiv) were added. A mixture of DMF:Dioxane: H_2O in the ratio of (9:6:1) respectively was prepared and 5.0 mL was added to each vial. Increasing concentrations of H_2TDC i.)0.113 g, 0.0007 mol, 0.5 equiv ii.) 0.226 g, 0.0001 mols, 1.0 equiv or iii.) 0.452 g, 0.003 mol, 2 equiv were added to the three different vials each prepared in triplicate for the three investigated temperature conditions, 60 ^{o}C, 100 ^{o}C, and 120 ^{o}C in respective ovens. This experiment was conducted in duplicate for each of the temperature conditions. After 24 hours of incubation, the sample was retrieved, cooled down

to room temperature, centrifuged at 5000 rpm for 10 minutes and decanted. This was repeated an additional two times with DMF (10 mL each). The sample was dried in the vacuum pump overnight for powder pattern analysis using the PXRD.

b) Using Terephthalic Acid (T.A) linker

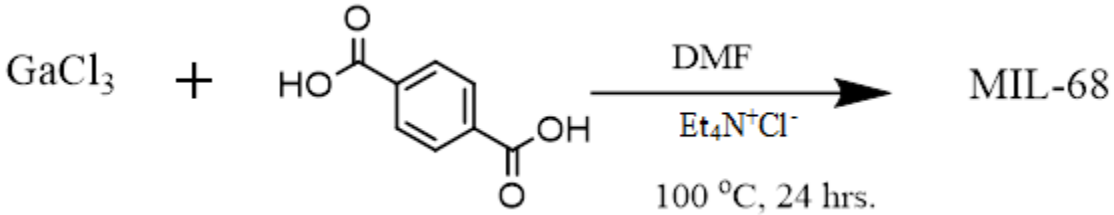

Figure 9: MOF synthesis using T.A. linker.

The experiment was conducted as in CAU-51 procedure above with the only change in the type of linker used. Into 3 vials 20 mL each, $GaCl_3$ (0.232 g, 0.0001 mol, 1 equiv) and $Et_4N^+Cl^-$ (0.186 g, 0.001mols, 1.2 equiv) were added. A mixture of DMF:Dioxane: H_2O in the ratio of (9:6:1) respectively was prepared and 5.0 mL was added to each vial. Three sets concentration of linker, terephthalic acid, i.) 0.110 g, 0.0007 mols, 0.5 equiv ii.) 0.219 g, 0.001mols, 1 equiv iii.) 0.439 g, 0.002 mol2, 2 equiv. This was prepared in duplicate for each of the three investigated temperature conditions, 60 °C, 100 °C, and 120 °C. After 24 hours of incubation, the sample was retrieved, cooled down to room temperature, centrifuged at 5000 rpm for 10 minutes and decanted. This was repeated an additional two times with DMF (10 mL each). The sample was dried in the vacuum pump overnight for powder pattern analysis using the PXRD. The product obtained matched MIL-68 powder pattern.

c) Using $Ga(NO_3)_3$

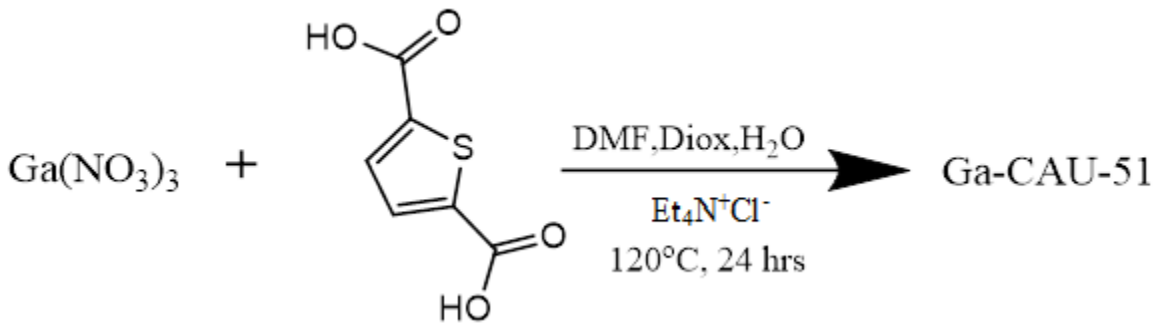

Figure 10: Ga-CAU-51 synthesis from $Ga(NO_3)_3$.

Into 3 vials 20 mL each, $Ga(NO_3)_3$ (0.256 g, 0.001 mol, 1 equiv) and $Et_4N^+Cl^-$ (0.186 g, 0.001s mol, 1.2 equiv) were added. A mixture of DMF: Dioxane: H_2O in the ratio of (9:6:1) respectively was prepared and 5.0 mL was added to each vial. Increasing concentrations of H_2TDC i.)0.113 g, 0.0007 mols, 0.5 equiv ii.) 0.226 g, 0.001 mols, 1.0 equiv iii.) 0.452 g, 0.002 mols, 2 equiv were added to the three different vials each prepared in triplicate for the three investigated temperature

conditions, 60 ºC, 100 ºC, and 120 ºC in respective ovens. This experiment was conducted in duplicate for each of the temperature conditions. After 24 hours of incubation, the sample was retrieved, cooled down to room temperature, centrifuged at 5000 rpm for 10 minutes and decanted. This was repeated an additional two times with DMF (10 mL each). The sample was dried in the vacuum pump overnight for powder pattern analysis using the PXRD resulted in large, circular, white crystalline product that matched Ga-CAU-51 powder pattern.

2.2.1.2 CAUMOF-11

i) Using $GaCl_3$ and Et_4NCl^-

Figure 11: CAUMOF-11 synthesis.

CAUMOF-11 was synthesized in line with the original synthesis procedure by Lee and group.[44] $GaCl_3$ and $Et_4N^+Cl^-$ were used in place of $Ga(NO_3)_3$ and tetrapropyl ammonium chloride ($Pr_4N^+Cl^-$) respectively. To a 20 mL vial $GaCl_3$ (0.350 g, 0.002 mol, 1 equiv) was dissolved in 5.0 mL DMF, $Et_4N^+Cl^-$ (0.330 g, 0.0002 mol, 1 equiv) was added to the solution followed by HNO_3 0.5 mL. The mixture was sonicated for 30 minutes. A solution of BTC (1,3,5-$C_6H_3(CO_2H)_3$) (0.400 g, 0.002 mol, 1 equiv) prepared in 5.0 mL DMF was then added slowly to the mixture. The mixture was set in duplicated autoclave at 180 ºC oven for three days. The sample was retrieved cooled and centrifuged at 5000 rpm for 10 minutes and decanted. The sample was then dried in the vacuum pump overnight followed by powder pattern analysis using the PXRD and a solid-state Raman.

ii) Using H_2TDC

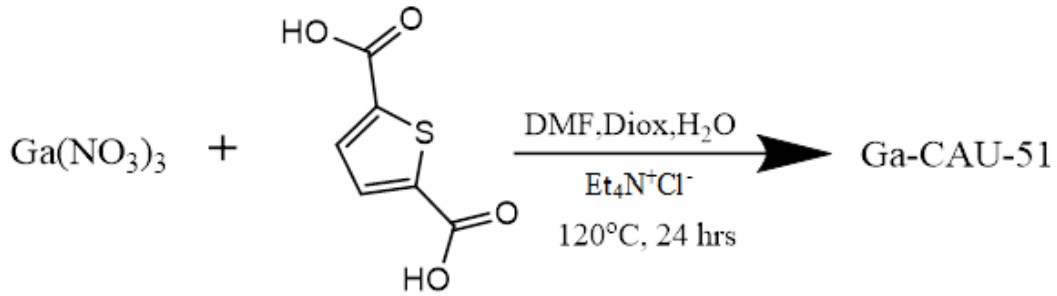

Figure 12: $GaCl_4EtN$ synthesized in new MOF attempt.

The reaction mixture was prepared following the CAUMOF-11 procedure. To a 20 mL vial $GaCl_3$ (0.350 g, 0.002 mol, 1 equiv) was dissolved in 5.0 mL DMF, $Et_4N^+Cl^-$ (0.330 g, 0.002 mol, 1 equiv) was added to the solution followed by HNO_3 0.5 mL. The mixture was sonicated for 30 minutes. A solution of H_2TDC (0.344g, 0.002 mol, 1 equiv) 5.0 mL DMF was then added slowly to the mixture. The mixture was prepared in duplicate and set in autoclaves at 180 ℃ oven for three days. The sample was retrieved cooled, centrifuged at 5000 rpm for 10 minutes and decanted. The sample was then dried in the vacuum pump overnight followed by powder pattern analysis using the PXRD and a solid-state Raman. The X-ray powder pattern matched $GaCl_4TEA$.

iii) Using dioxane: toluene solvent

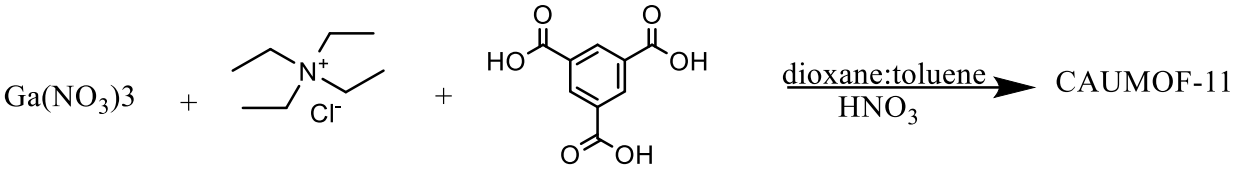

Figure 13: CAUMOF-11 synthesis in dioxane: toluene mixed solvent system

The reaction mixture was prepared following the CAUMOF-11 procedure. To a 20 mL vial $GaCl_3$ (0.350 g, 0.002 mol, 1 equiv) was dissolved in 5.0 mL dioxane:toluene 1:1, $Et_4N^+Cl^-$ (0.330 g, 0.002 mol, 1 equiv) was added to the solution followed by HNO_3 0.50 mL. The mixture was sonicated for 30 minutes. A solution of H_2TDC (0.344g, 0.002 mol, 1 equiv) 5 mL dioxane:toluene,1:1 was then added slowly to the mixture. The mixture was prepared in duplicate and set in autoclaves at 180 ℃ oven for three days. The sample was retrieved cooled, centrifuged at 5000 rpm for 10 minutes and decanted. The sample was then dried in the vacuum pump overnight followed by powder pattern analysis using the PXRD and a solid-state Raman. The X-ray powder pattern matched CAUMOF-11.

2.2.2 $GaCl_4^-$ synthesis

As shown in 2.2.1.2 (ii) above, attempt to synthesize Ga-MOF with H_2TDC under CAUMOF-11 conditions yielded $GaCl_4TEA$ in impure form since it did not meet all the known chemical characteristics besides matching the PXRD description. To understand this product's role in Ga-MOF synthesis, we decided to produce it in the pure form for experimental manipulations like new MOF attempt both synthesis and *in situ* solvation characterization.

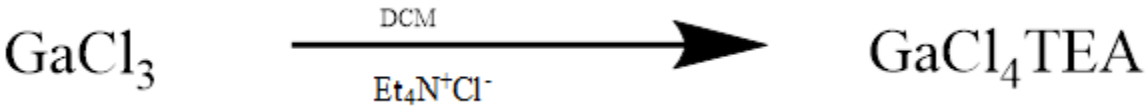

Figure 14: $GaCl_4^-$ synthesis in DCM

$GaCl_4TEA$ was synthesized according to the Schmulbach procedure.[44,45] In a 50.0 mL Elenmeyer flask, $GaCl_3$ (1.381 g, 0.008 mol, 1 equiv) was dissolved in 5.0 mL dichloromethane (DCM). $Et_4N^+Cl^-$ (1.256 g, 0.008 mol, 1 equiv) were dissolved in 20.0 mL DCM and added to the $GaCl_3$ solution dropwise at room temperature. The product formation was observed in the build-up of white crystals. The solvent was evaporated for 20 minutes over a 30 ℃ water bath then was slowly

cooled at room temperature and eventually in ice. Excess solvent was removed and the sample dried in a vacuum pump. The salt was recrystallized in fresh DCM and vacuum dried. PXRD and solid-state Raman confirmed the structure. $GaCl_4$TEA was then recultivated in the CAUMOF-11 attempt.

2.2.2.1 $GaCl_4^-$ for MOF synthesis with trimesic acid.

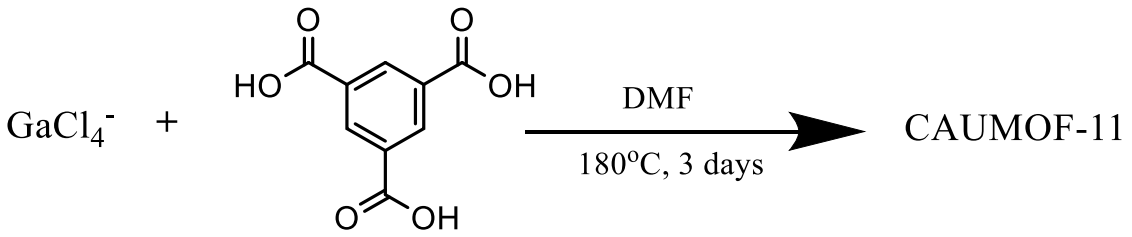

Figure 15: CAUMOF-11 synthesis from $GaCl_4^-$.

In a 20 mL vial, $GaCl_4^-$ (0.358 g, 0.002 mol, 1 equiv) was dissolved in 5.0 mL DMF. (0.714 g, 0.003 mol, 2 equiv) of BTC in 5 mL DMF solution was then added slowly to the mixture. This was done in duplicate and then incubated for 3 days at 180 ºC. The crystalline product was centrifuged followed by two DMF washes and then dried. A few crystals were crushed for PXRD.

2.2.2.2 $GaCl_3$ + $GaCl_4^-$ in DMF and THF

$GaCl_3$ (0.088 g, 0.001 mmols, 1 equiv) was dissolved in 5ml DMF in a 20.0 mL vial and set up for Raman for half an hour. 5.0 mL of $GaCl_4^-$ (0.240 g, 0.001 mol, 1 equiv) solution DMF was then added and run for 30 minutes before increasing temperature to 65 degrees. The experiment was repeated with THF solvent and scans were collected.

2.2.2.3 $GaCl_4^-$ in THF and DMF

$GaCl_4^-$ (0.240 g, 0.001mol,) was weighed into a 20.0 mL vial and to it, 5.0 mL of THF was added to dissolve into a colorless solution. The vial was sealed with Teflon lined cap and set up for Raman at room temperature and 65 degrees heat for 1 hour each in the conditions. The same experiment was repeated for DMF and Raman's scans collected.

2.2.3 $Et_4N^+Cl^-$ in DMF

$Et_4N^+Cl^-$ (0.800 g, 0.005 mol) was dissolved in 5.0 mL DMF and set up for Raman at room temperature and at 65 °C for one hour exposure. The data obtained were analyzed in MATLAB.

2.2.3.1 $GaCl_3$ + $Et_4N^+Cl^-$ in DMF

0.232 g of GaCl3 (0.230 g, 0.001 mmols, 1 equiv) were dissolved in 5.0 mL DMF in a 20.0 mL vial. $Et_4N^+Cl^-$ (0.440 g, 0.003 mol, 2 equiv) were added to the solution. The vial was heated at 100 °C and reaction monitored for 24 hours in Raman. The collected data was analyzed in MATLAB.

2.3 Computations; Ionization and solvation of $GaCl_3$ and $Ga(NO_3)_3$ in organic solvents (DMF, Acetone, dioxane, THF, NMP)

The energy of solvation was calculated for $GaCl_3$ and $Ga(NO_3)_3$ in the different organic solvents as mono-solvents built-in Spartan followed by geometry optimization in Q-Chem. Enthalpy calculations were then done for comparison across the different solvents and with *in situ* Raman findings.

2.3.1 *in situ* Raman analysis for CAUMOF-11 from $GaCl_3$ and CAUMOF-11 from $Ga(NO_3)_3$ synthesis.

MOF synthesis mixture for the two was prepared as in **2.2.1.2 i**) above and the reaction was set up in Raman at 120 ℃ for 5 days. Scans were taken, 10 accumulations each two exposures with 15 minutes intervals for 5 days. 474 time points were collected and analyzed in MATLAB.

2.3.2 Solvation of $GaCl_3$ in (DMF, Acetone, dioxane, tetrahydrofuran (THF), n-methylpyrolidone (NMP) and toluene (mono and mixed solvents).

$GaCl_3$ (0.880 g, 1.0 mmol) was dissolved completely in 5 mL organic solvents and set up in the sand bath for analysis in the Raman oven (dark box). A lower concentration of $GaCl_3$ (0.880 g, 0.1 mmol) was used for THF solvent due to fluorescence at higher concentrations. They were run for 1 hour each at room temperature and 65 ℃ with 2 minutes scan intervals, 2-second exposure, and 10 accumulations. The data was then an analyzed in Matlab.

Note: Mixed solvent systems were in a ratio of 1:1. (DMF:THF, THF:Toluene, NMP:DMF, Dioxane:Toluene).

2.3.2.1 Solid state Raman

0.100 g solids from CAUMOF-11, $Ga(NO_3)_3$ $GaCl_3$, $GaCl_4^-$, $Et_4N^+Cl^-$, were separately crushed to a fine powder and placed in aluminum lined vial caps. Single scans were taken with the sample under the Raman probe, followed by data analyzed in MATLAB.

CHAPTER III: RESULTS AND DISCUSSION

As mentioned previously, there are very few Ga-MOFs described in literature with a single anionic MOF. Our starting point was to synthesize CAUMOF-11 and CAU-51 under the original synthesis conditions and later alter the inputs; linker, metal source, single solvent and mixed solvent systems to explore the parameters necessary for successful synthesis, while monitoring the reaction progress *in situ*. From this information, our goal was to develop a synthesis of new MOF material while building our understanding of Ga-MOF synthesis with a focus on determining the structure of solution-phase inorganic Ga-starting materials.

Solvents play an important role in solvothermal syntheses and their dielectric constant determine the solvation of starting materials to enable progression of reaction and subsequent formation and isolation of product. The higher the solubility of the reactants the better the MOF outcomes. Coordination of solvent to the metal center also facilitates for possible transformations for example ionization in the reaction progression.

Reproducing the known Ga-MOFs under the original synthesis conditions, described by Stock and Lee, provided the starting materials for this work. The products were subsequently reproduced while observing the process in situ and outcomes were analyzed using PXRD and solid-state Raman. In situ Raman solvation of the starting material was also monitored to determine the starting point in Ga-MOF synthesis.

3.1 Gallium MOFs (CAU-51 and CAUMOF-11)

Using the previously described procedure by Stock and co-workers,[13] with $GaCl_3$ in place of $Ga(NO_3)_3$, CAU-51 was synthesized by Joseph Strozier more than seven years ago in the Genna lab. We reproduced the MOF following the Strozier's procedure. Quality MOF crystals were derived from reactions involving half equivalents of linker as starting material. The synthesized product matched the calculated powder pattern for Ga-CAU-51 plotted in a diffractogram. Ga-CAU-51 is characterized by presence of 4 major PXRD reflections at 2 Θ= 9, 11,13 &16, Figure 16.

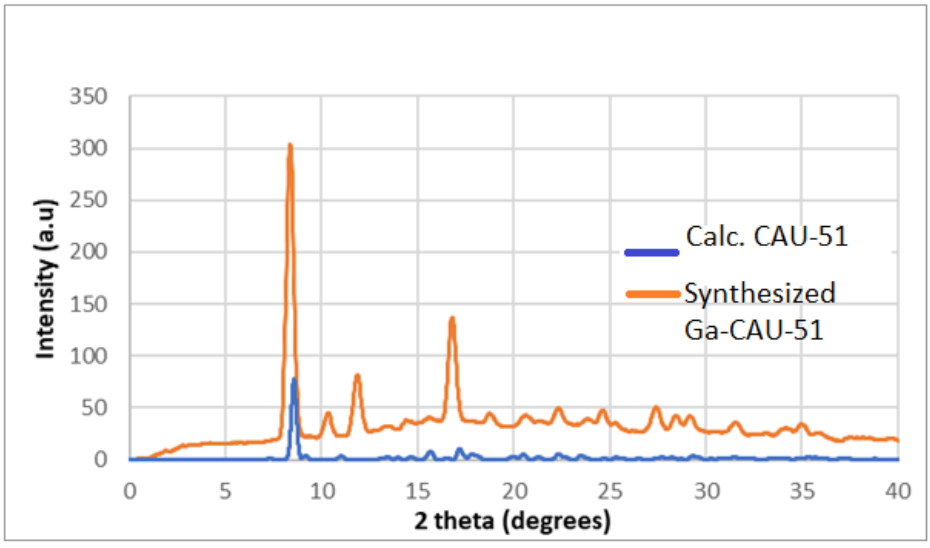

Figure 16: PXRD diffractogram of synthesized Ga-CAU-51 and calculated CAU-51 PXRD pattern.

Under similar conditions for synthesis, as described by Lee and coworkers, replacing $Ga(NO_3)_3$ and PrN^+Cl^- with $GaCl_3$ and $Et_4N^+Cl^-$ respectively, resulted in the CAUMOF-11. CAUMOF-11 crystals are circular with an average width of 0.8 mm. To obtain the X-ray powder pattern, the crystals were crushed to fine powder and the derived diffractogram was characterized by five major reflections at 2Θ =11°,16°, 18°,20° and 21°and matched the calculated powder pattern for the calculated MOF, Figure 17.

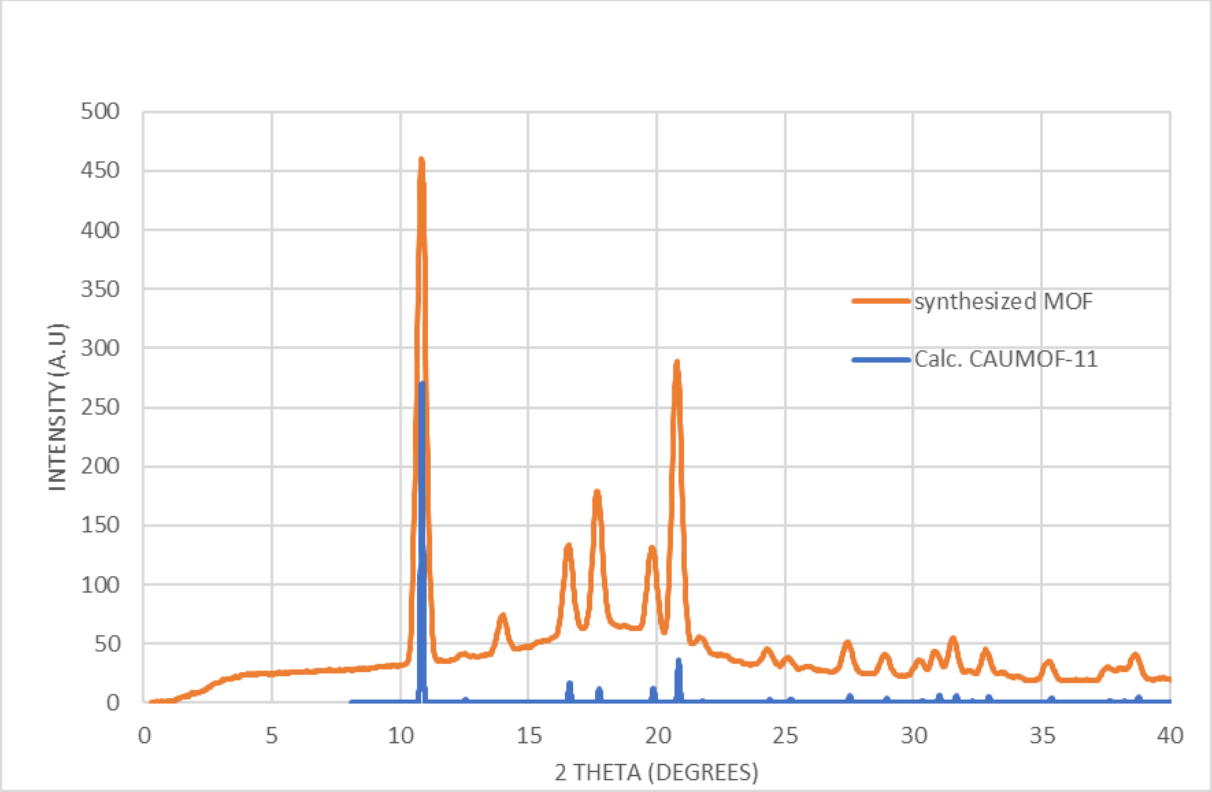

Figure 17: PXRD diffractogram for synthesized CAUMOF-11 and calculated CAUMOF-11 PXRD pattern.

Since the two metal sources were interchangeable for the synthesis of CAU-51 and CAUMOF-11, we made a hypothesis that they must be chemically evolving into a common intermediate to result in a similar product. Using CAUMOF-11, we monitored the synthesis over a period of five days to identify significant chemical changes taking place in the reaction as it progressed to form product. This was done in separate reactions involving either $Ga(NO_3)_3$ or $GaCl_3$ as the metal source, under same reaction conditions.

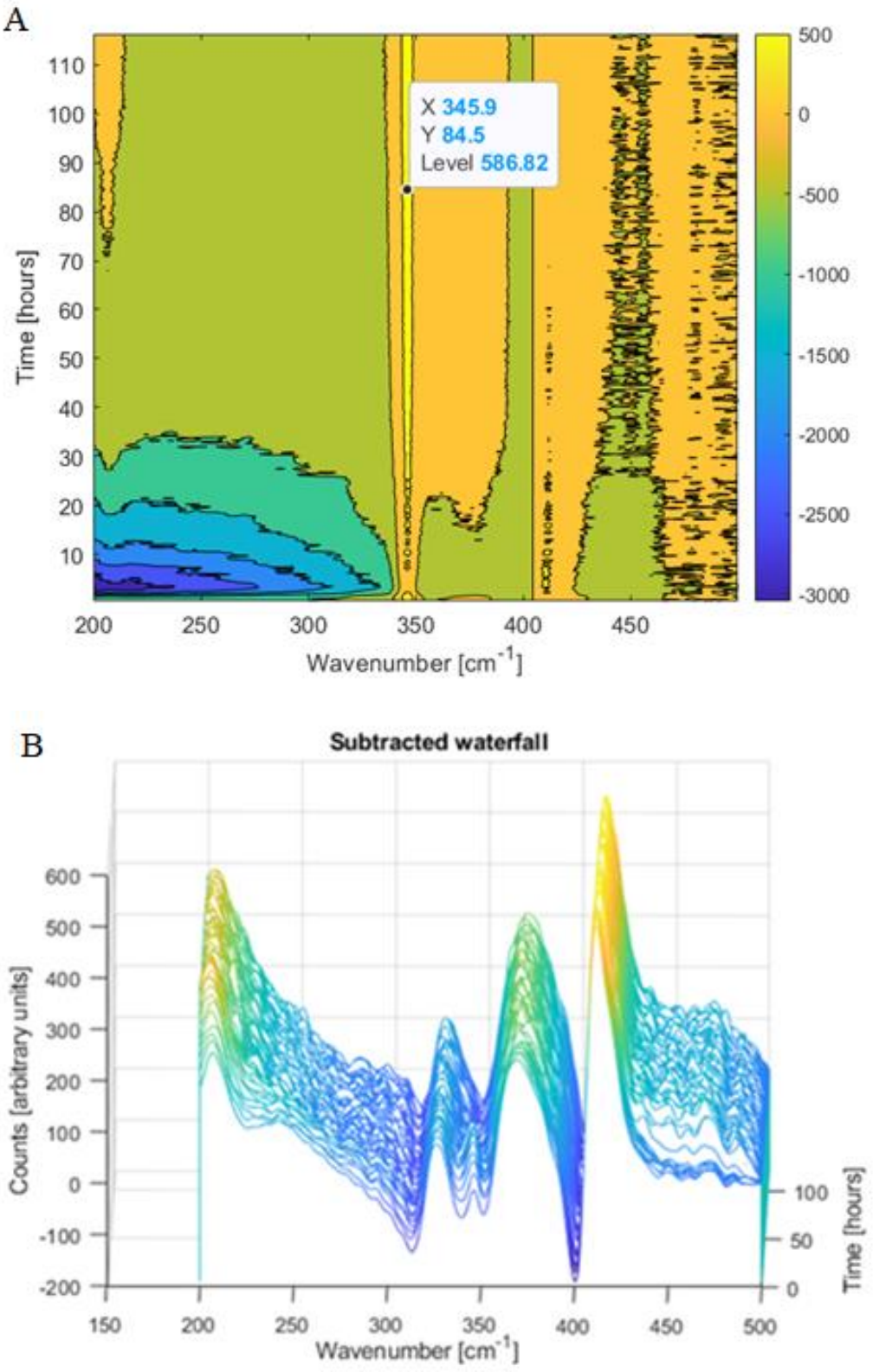

Figure 18: Contour and waterfall graphs for CAUMOF-11. A; from $GaCl_3$. B; from $Ga(NO_3)_3$. Unconsumed peak at 345 cm^{-1}.

The *in situ* Raman for CAUMOF-11 synthesized from $Ga(NO_3)_3$ in the presence of $Et_4N^+Cl^-$, showed a peak at 345 cm^{-1} similar to the synthesis with $GaCl_3$ (Figure 18). Although the peak in the $Ga(NO_3)_3$ reaction is not as prominent as the peak in $GaCl_3$ reaction, which we assume represents the same intermediate, the product endpoint is achieved.

By virtue of a nitrate and a chloride resulting in the same MOF product under the same conditions, insinuates that they evolve into common intermediates within the MOF synthesis to result in CAU-51 and CAUMOF-11. $Ga(NO_3)_3$ is believed to easily take up a free chloride available in solution, as provided by $Et_4N^+Cl^-$ / $Pr_4N^+Cl^-$, to form $GaCl_4^-$ (Figure 19). This is a feasible reaction favored forward by its' exothermic nature.

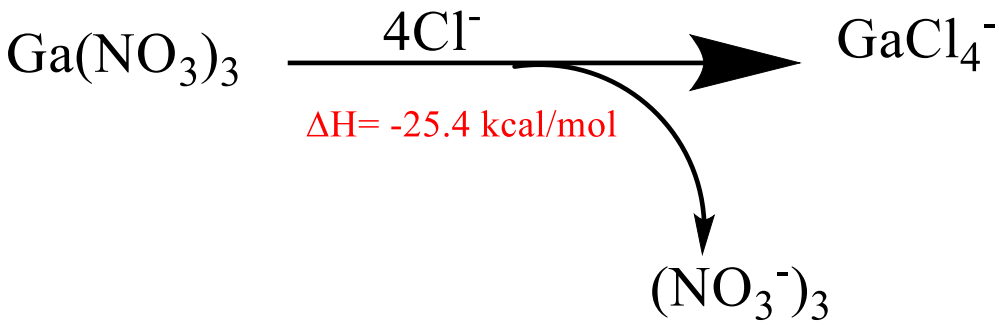

Figure 19: Formation of $GaCl_4^-$ in MOF synthesis reactions involving Ga^{3+}.

Having confirmed that the synthesis conditions and materials available could lead to the production of our MOFs of interest, we set out to experiment on possible outcomes of different inputs on the MOF synthesis. Different linkers have unique geometry largely influenced by their topicity, composition and size that play a role in the MOF type, structure and chemical composition. The original linker in CAU-51 synthesis is H_2TDC and attempts with terephthalic acid linker in similar conditions, yielded MIL-68, both of which are neutral infinite chain MOFs, Figure 20. MIL-68 is a MOF that has been synthesized with a number of metals, including Fe, Al, V, In and Ga.

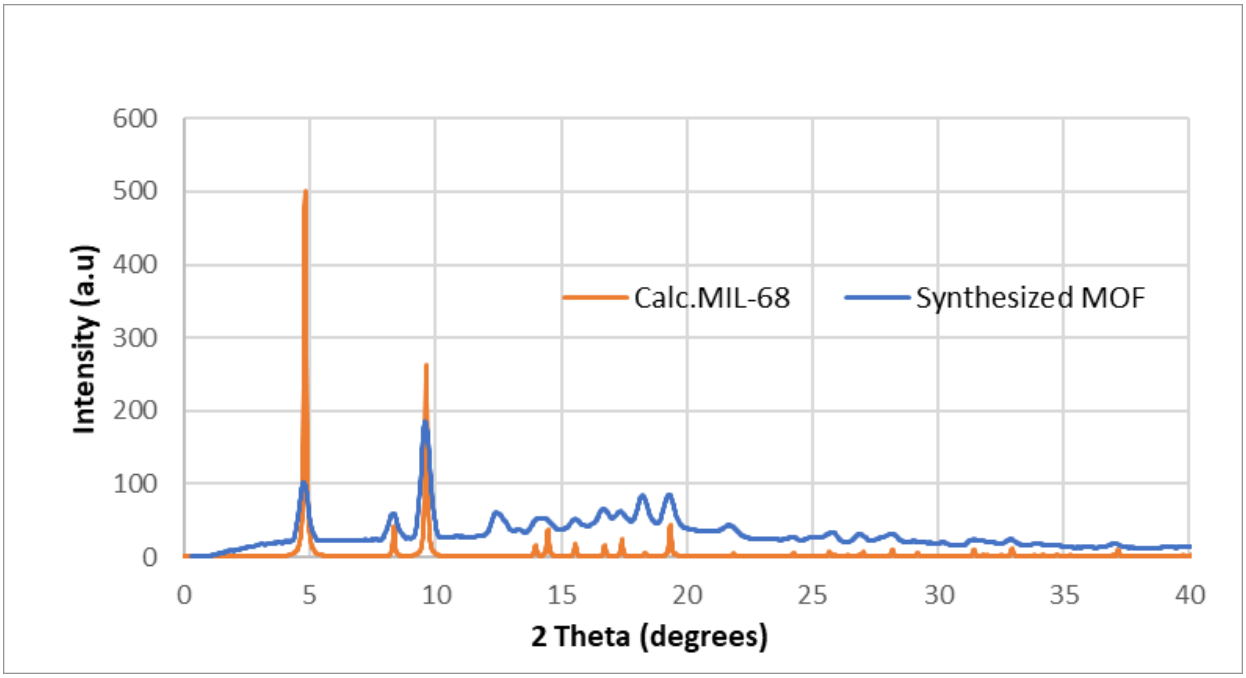

Figure 20: PXRD diffractogram of the synthesized MOF matching the calculated MIL-68 pattern.

DMF is the most commonly used solvent in MOF synthesis. Besides solubilizing reagents, some solvents like DMF also provides charge balancing cations to the reaction. In most cases, highly polar solvents are preferred and there are hardly any studies in literature on the role of other solvents like toluene and dioxane that are low in polarity index. Attempts to synthesize MOF with a toluene:dioxane mixture in a 1:1 ratio in suitable reaction conditions resulted in crystalline CAUMOF-11 product. Toluene is known not to coordinate metals due to its chemical structure. Dioxane has a low dielectric constant hence low solubility of compounds. This shows that DMF and other highly polar solvents aren't necessary for making CAUMOF-11.

MOF synthesis attempts using H_2TDC under CAUMOF-11 conditions yielded $GaCl_4[Et_4N]$ which was isolated as pale-yellow pellets and the powder was analyzed using PXRD (Figure 21). For the first time in our synthesis explorations, we isolated a non-MOF material that we were able to characterize. We hypothesized that it is an important intermediate or perhaps a side product whose role in MOF synthesis we are yet to determine. It has been reported in the literature that $[GaCl_4]^-$ in solution can exist as an un-solvated anion or di-solvated anion and enthalpy calculations *in silico* have shown that its occurrence in the MOF synthesis pathway is enthalpically feasible.[46] Similarly, *in situ,* Raman solvation analysis in polar solvents has supported the presence of either of the anions as indicated by the intense Raman bands at 345 cm^{-1}.

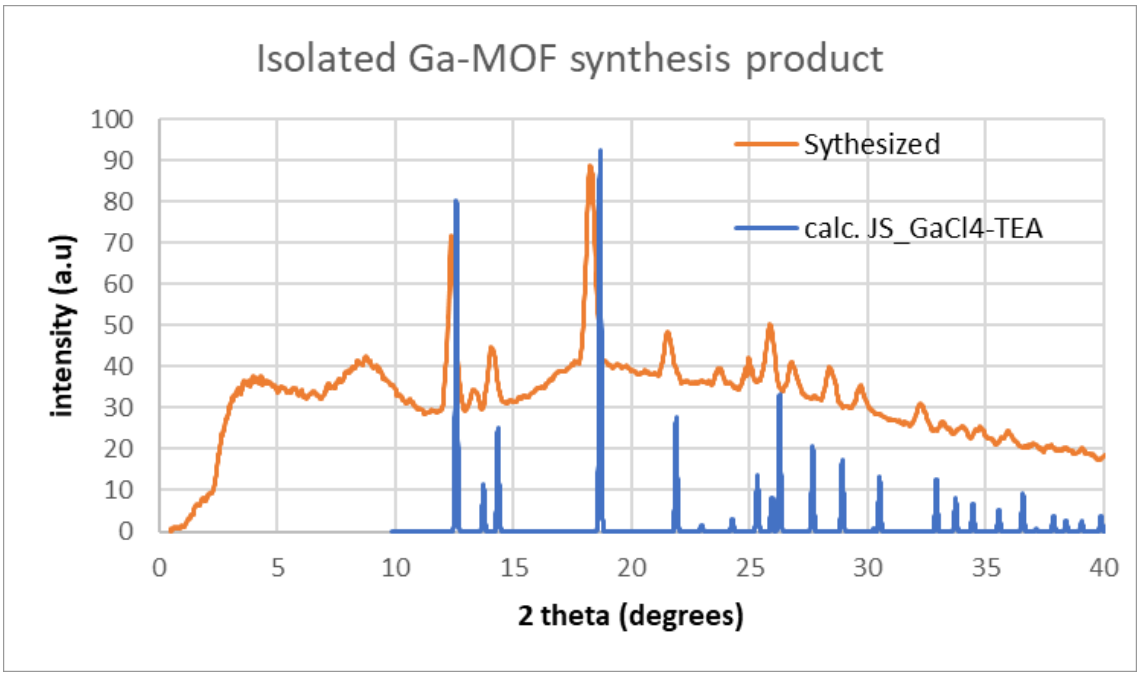

Figure 21: Diffractogram for isolated $GaCl_4TEA$ by-product.

We decided to monitor the CAUMOF-11 synthesis using *in situ* Raman in order to account for the isolated product. This reaction was monitored over a period of five days, two days longer than the established period, due to the changes in the CAUMOF-11 synthesis conditions (temperature and pressure) to suit the provisions of the Raman. Analysis of the data showed a band at 345 cm^{-1} that forms immediately after the reaction is started. Two other bands appear: one at 1035 cm^{-1}, forms as the reaction progresses and 1039 cm^{-1} that forms some hours into the reaction but starts to be consumed at more than 30 hours as the reaction progresses, Figure 22 A and B.

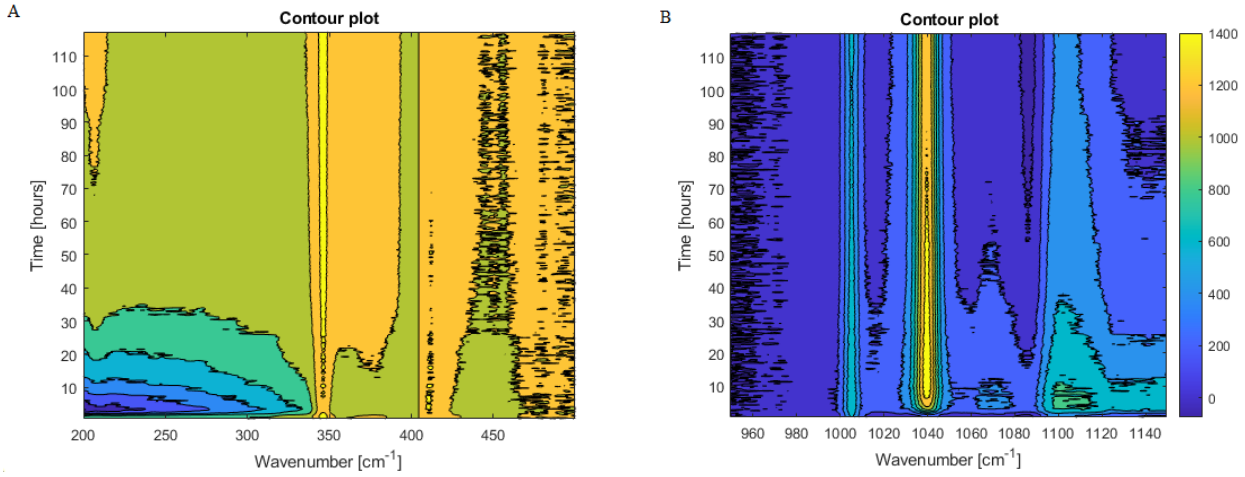

Figure 22: Contour plots for *in situ* CAUMOF-11 synthesis. A) 347 cm^{-1}. B) 1039 cm^{-1} peaks.

Integration of two bands 345 cm^{-1} and 1035 cm^{-1} gives more insight to what is taking place. Figure 23, shows a decline in a phase, blue curve, as another phase increases, orange curve, with time during the CAUMOF-11 synthesis. We made a hypothesis that the declining phases represent

possible intermediates in CAUMOF-11 synthesis that get consumed in the reaction as the crystalline product material is accumulated over time, rising phase. Solid-state Raman and PXRD confirmed the identity of the product which matched the CAUMOF-11 and has a peak represented by a small hump at 1035 cm^{-1}, Figure 24. The declining phase represented by the Raman band at 1039 cm^{-1} requires further characterization.

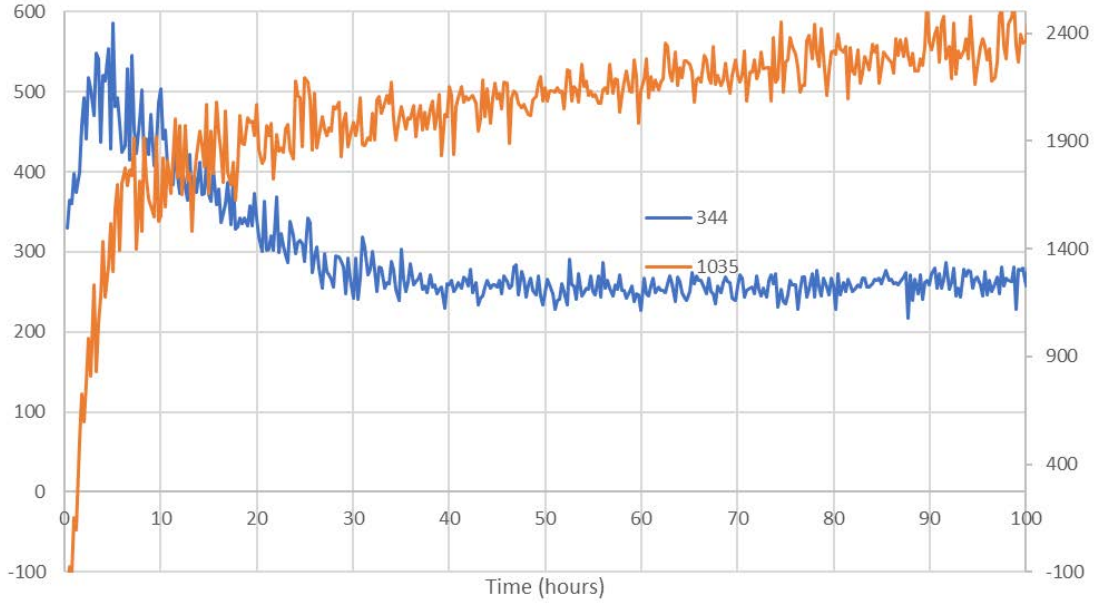

Figure 23: Integrated conspicuous phases of CAUMOF-11.

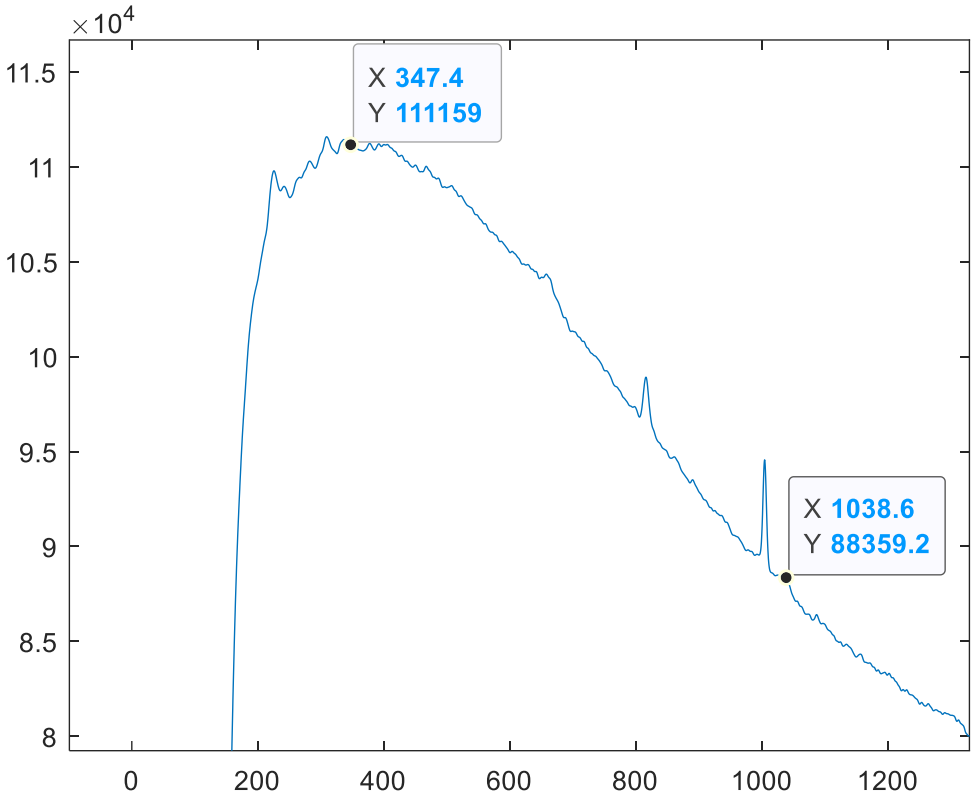

Figure 24: Solid-state Raman for CAUMOF-11.

Identity for the peaks that stood out in the *in situ* Raman analysis remains to be affirmed. We know, from other MOFs that have been studied, that several intermediates are involved in the synthesis of crystalline material, whereby some are almost identical thus difficult to differentiate without isolating them synthetically for characterization. We decided to do an exemplary roadmap for a Ga-MOF synthesis to gain insight on the transformations taking place in the synthesis. Starting from $GaCl_3$(DMF), we ended up forming a known tetrahedral node for anionic Ga-MOFs, $[Ga(COOH)_4]^-$, through two downhill pathways illustrated in Figure 25. Figure 26 energy graph expounds on the clear nature of reactions.

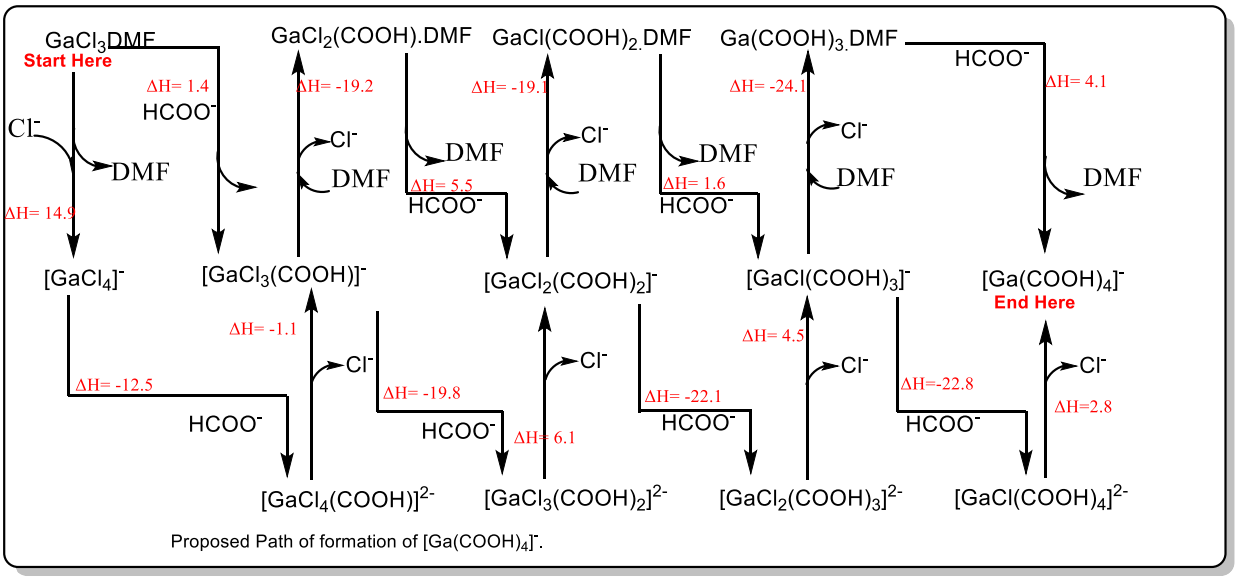

Figure 25: Ga-MOF intermediates.

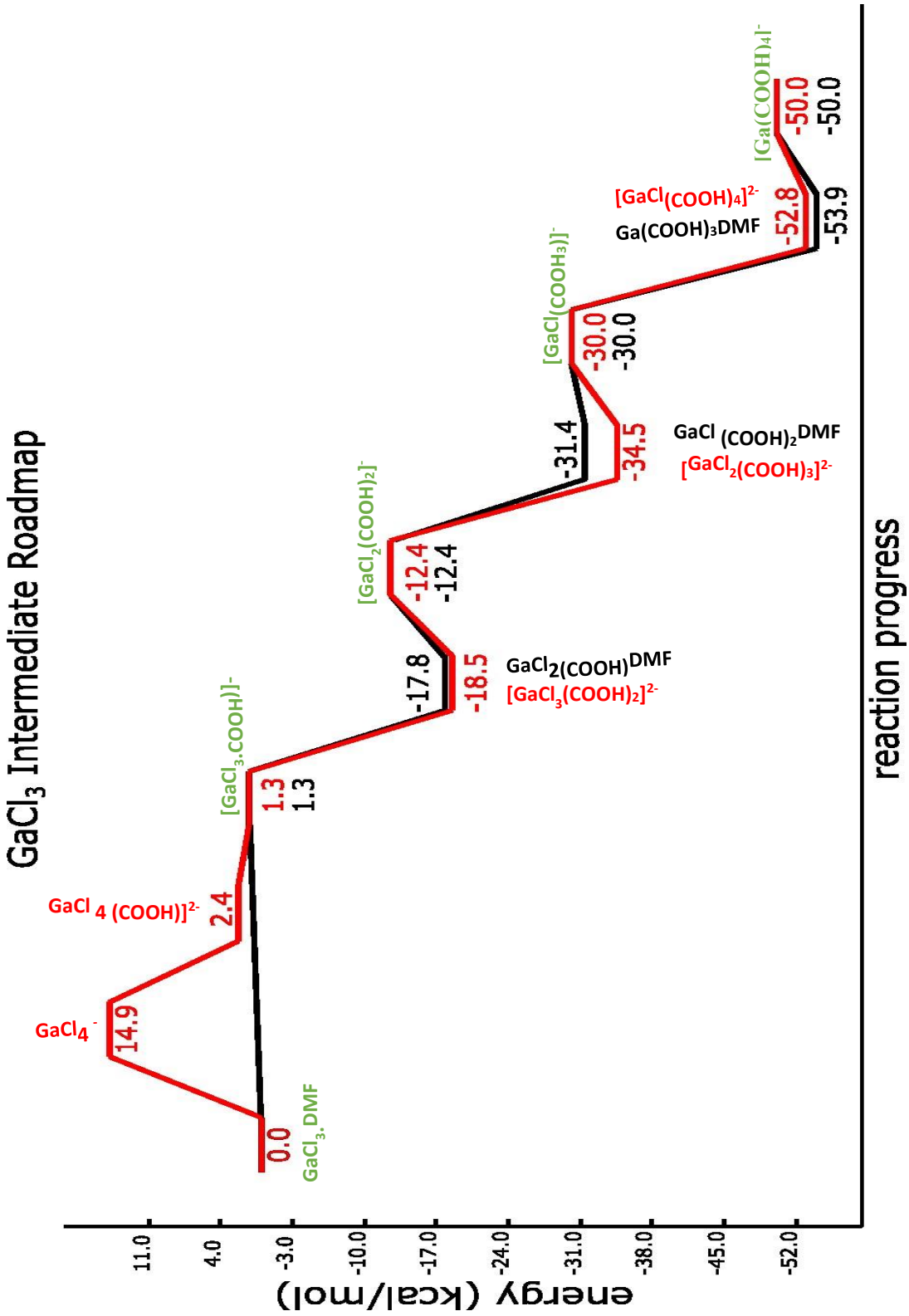

Figure 26: Simplified energy graph roadmap for Ga-MOF synthesis.

The roadmap was developed from the enthalpy calculations of the $GaCl_3$ reaction with formate groups as optimized in Q-chem. The intermediates shown are a result of the addition of formate ($HCOO^-$) at the expense of chloride as would be the case in Ga-MOF synthesis using the terephthalic acid linker. Represented are the two different pathways; in red and black as described by the first intermediate formed and the enthalpic favorability. The intermediates have a stable tetrahedral structure, for the neutral and monanionic (common) pathway, and an octahedral geometry for the dianionic pathway. Formed at the end of the pathways is a common intermediate that is a known node for anionic Ga-MOFs, tetrahedral $[Ga(COOH)_4]^-$.

One pathway (red) involves the formation of $GaCl_4^-$ as the first intermediate from solvated monomer, $GaCl_3$.DMF, and the ionizing atom being a free chloride as per the reaction below. The energy involved insinuates an uphill reaction involving a loss of DMF ligand. The other pathway, represented in black, starts off with a down-hill step to form the first common intermediate of the two pathways.

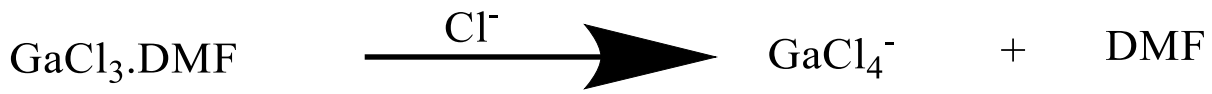

Figure 27: Ionization of $GaCl_3$ as calculated in the roadmap.

The uphill ionization may or may not be the ideal situation happening since we based our $GaCl_4^-$ formation on the monomer, yet $GaCl_3$ is available commercially as a dimer molecule Ga_2Cl_6, Figure 28. It can dissociate in solution to form its monomer state and that's where we based our calculations and analyses. More studies towards the understanding of the dimer at the starting point are recommended, otherwise the two pathways on the roadmap are both feasible in anionic MOF synthesis.

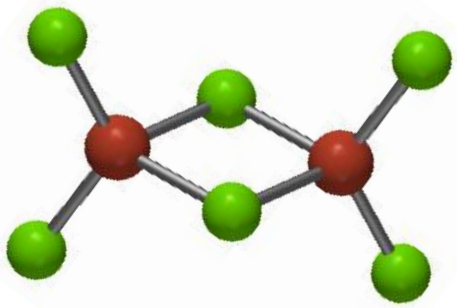

Figure 28: $GaCl_3$ dimer.

Previously, in the attempt to synthesize MOF, $GaCl_4TEA$ was isolated, and we hypothesized it to be an intermediate/side product that occurs at some point in the reaction but whose role was yet to be determined. The road map also supported its formation. We decided to run experiments on $GaCl_4TEA$ to learn more about its role in anionic MOFs synthesis. Schmulbach and co-workers' procedure enabled fast and high yield, 87%, production of this starting material.[45] *In situ* solvation analyses and MOF synthesis attempt experiments with $GaCl_4TEA$ gave more insights on the earlier findings.

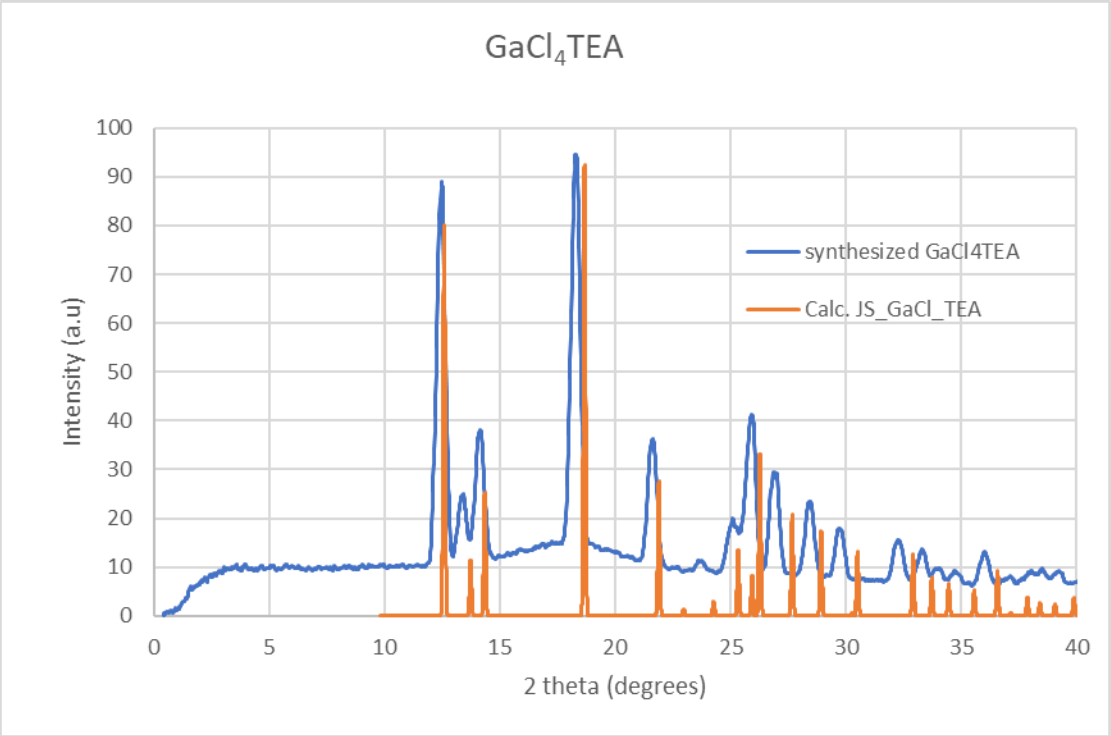

Figure 29: Diffractogram for synthesized $GaCl_4$.TEA using the Schmulbach's method.

According to Schmulbach, $GaCl_4TEA$ has a solid-state IR vibration peak at 372 cm^{-1}. We made a hypothesis that solvation and MOF synthesis attempts with $GaCl_4TEA$ will give us the true identity of the nature of the isolated Ga-intermediate and its role in MOF synthesis. The 345 cm^{-1} Raman band was found to be present in the solvation of synthesized $GaCl_4TEA$ analyses *in situ* in each of the organic solvents; DMF, NMP and THF, Figure 30.

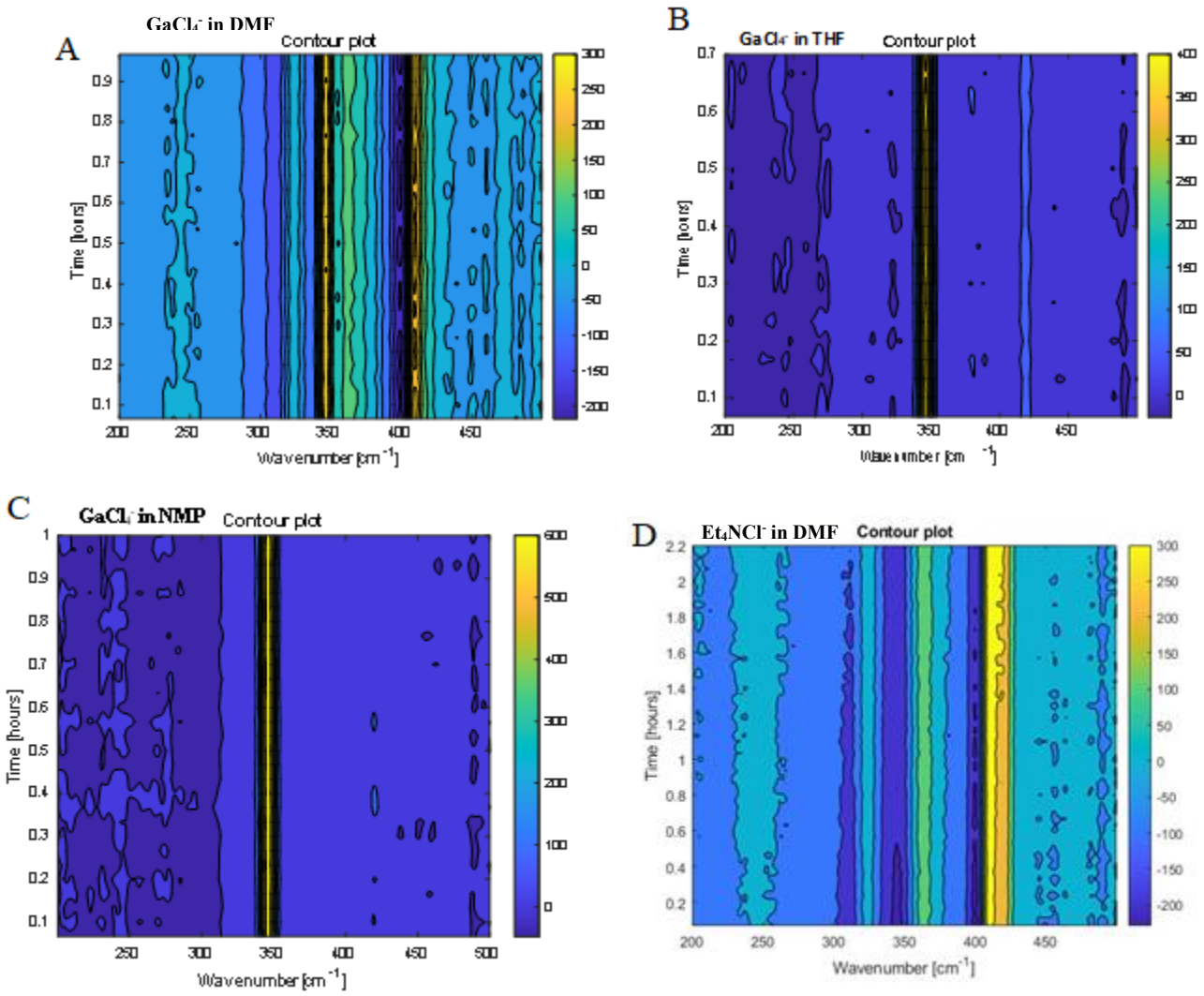

Figure 30: A, $GaCl_4TEA$ in DMF. B, $GaCl_4^-$ THF. C, $GaCl_4^-$ in NMP and D, $Et_4N^+Cl^-$ in DMF.

In DMF, the $GaCl_4^-$ forms two Raman bands at 345 cm^{-1} and 410 cm^{-1}. NMP has a high dielectric constant similar to DMF but only a single band is formed. We expect that the molecule, upon solvation in either of the solvents, to behave in a similar manner and so the reason for this discrepancy is yet to be determined. THF gave a single Raman band at 345 cm^{-1}. *In situ* Raman for $Et_4N^+Cl^-$ in DMF, both at room and elevated temperatures, confirmed the 410 cm-1 Raman band as representative of the compound, Figure 31. Since the tetrachloride salt occurs as $GaCl_4TEA$ upon synthesis, it was hypothesized that the tetraethyl ammonium is accounted for by the second Raman band observed in DMF. However, the reason why the second band is not occurring in the other organic solvents is yet to be determined. Perhaps solvation analysis of TEA in other organic solvents will help unravel this.

$GaCl_4TEA$ reaction with trimesic acid in DMF produced CAUMOF-11 (Figure 31). This is indicative of the important role it plays in its unsolvated form in anionic MOF synthesis. At this

point, the 345 cm^{-1} can confidently said to represent unsolvated $GaCl_4^-$. There are cases where vibrational frequencies of same compound observed under different spectroscopy machines gives different peaks. The pioneering studies on $GaCl_4$TEA synthesis and characterization gave an IR peak at 372 cm^{-1}.[45] Our Raman analysis of the same product, unsolvated $GaCl_4$TEA gave a peak at a different wave number and we attribute this to observing different vibrations that relate to Ga-Cl bond. However, more clarification can be made on this with additional studies.

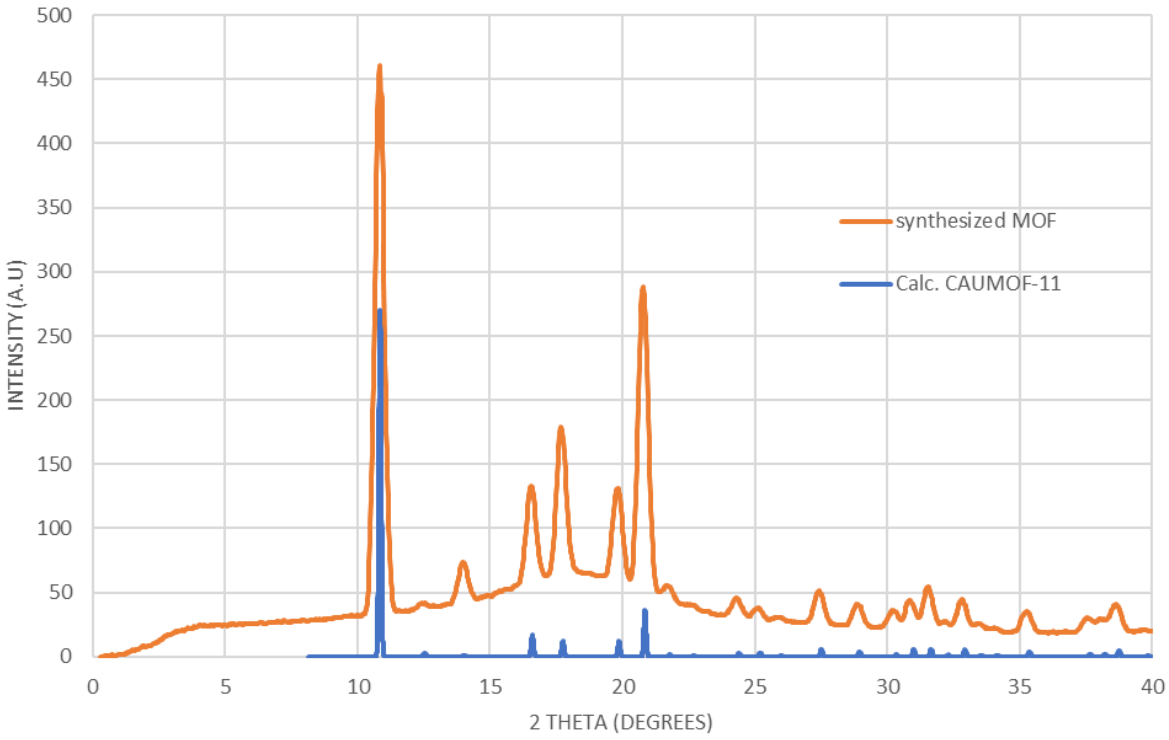

Figure 31: PXRD for CAUMOF-11 from $GaCl_4^-$ + BTC.

3.2 Solvation analysis of starting material.

To further understand the starting point for MOF synthesis, we looked into solvation analysis of starting materials as is the case in solvothermal synthesis. This is an important step in MOF synthesis as it facilitates the ligand exchanges that enable the transition through the possible phases that result in building units necessary for coordination into a material of good structural integrity. When $GaCl_3$ interacts with a solvent, it is likely to undergo solvation first with coordination of a maximum of three solvent ligands which is enthalpically favored as shown in the energy bar graphs, A, B and C in Figure 32. The ΔH was arrived at using DFT calculations post Q-chem optimization.

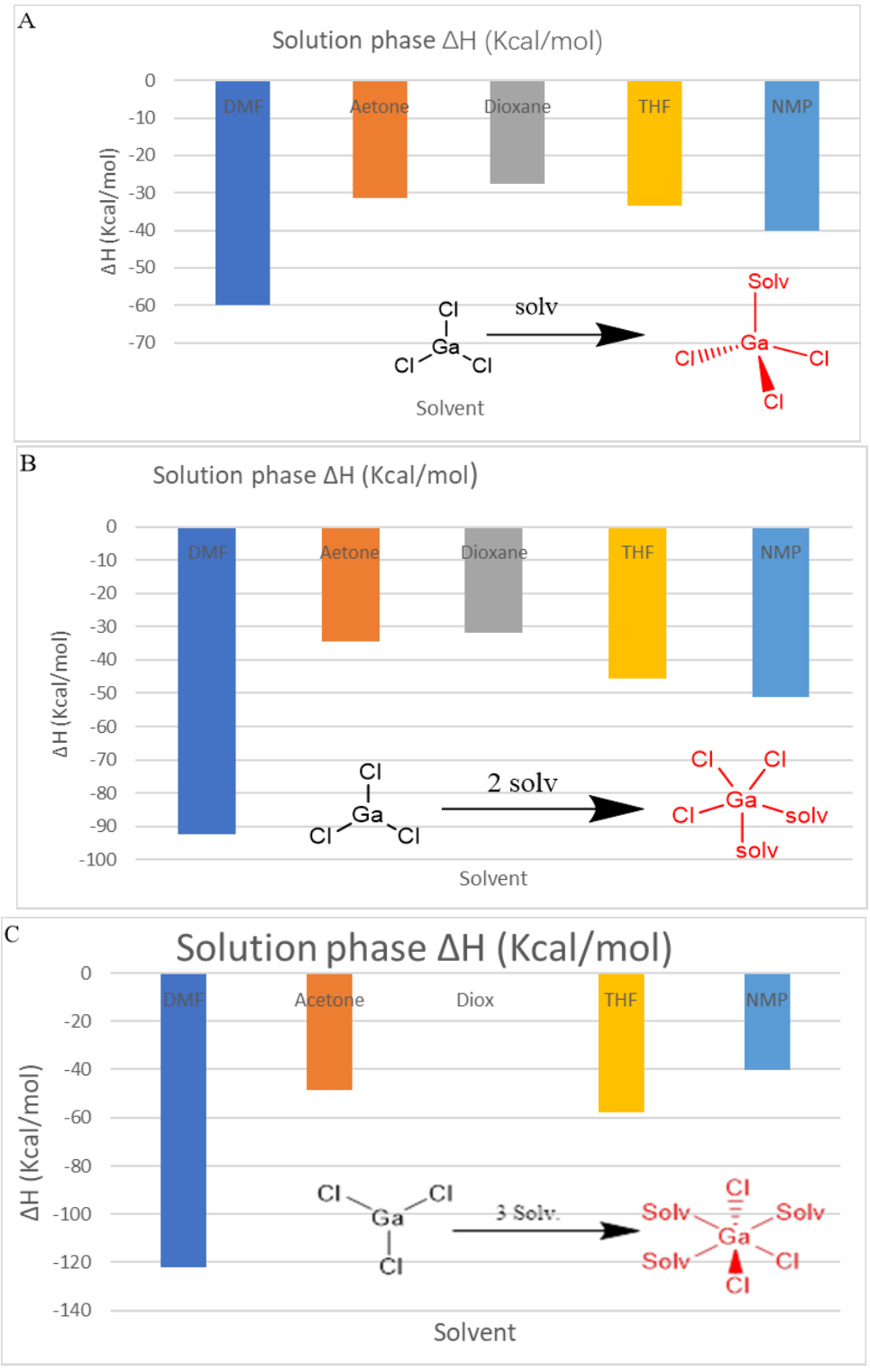

Figure 32: $GaCl_3$ in organic solvents. A, mono-solvate, B di-solvate, C tri-solvate.

Tri-solvate, trigonal bipyramidal gallium chloride is enthalpically most favored but is unstable as ionization occurs a lot more easily. We observed that dioxane disfavors the solvation of the two

Ga^{3+} metal sources and thus slows down the process of self-assembly.[1] DMF was found to be highly in favor of the dissolution process, by the enthalpy calculations.

The ionization of $GaCl_3$ to $GaCl_4^-$ is a possibility that happens almost effortlessly in some solvents like DMF while it is unlikely to occur in others. Enthalpically, ionization is most favored after the coordination of three solvent ligands. The chemical change was analyzed further using DFT calculations that gave enthalpy values that favored the formation of $GaCl_4^-$ that takes two forms, unsolvated or disolvate. Figure 33 A, B & C.

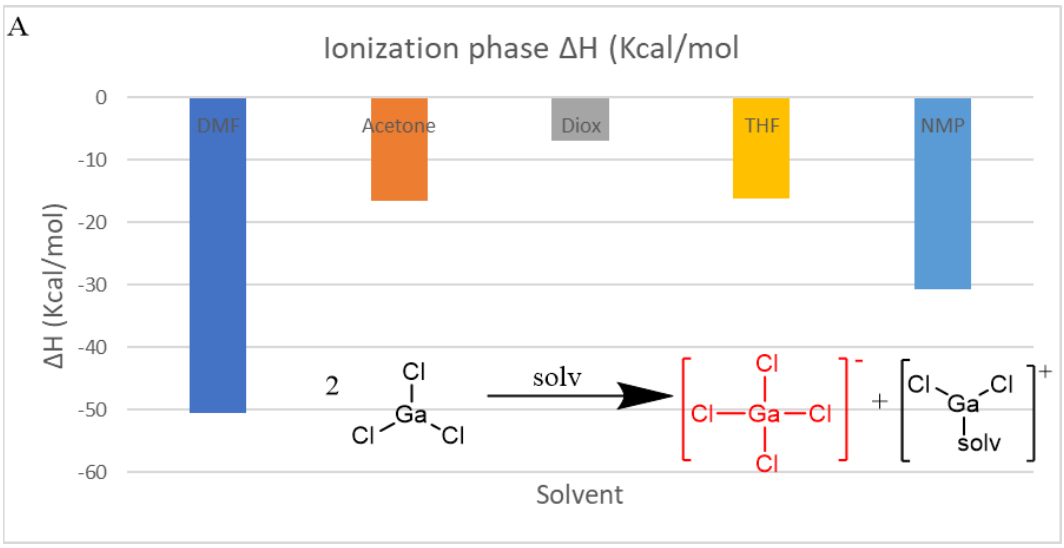

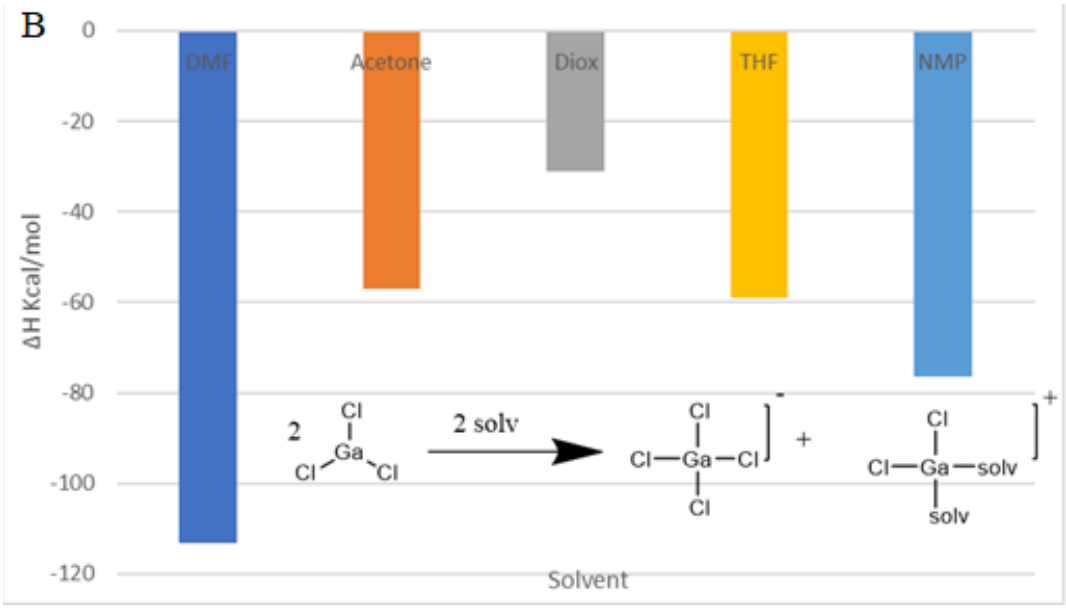

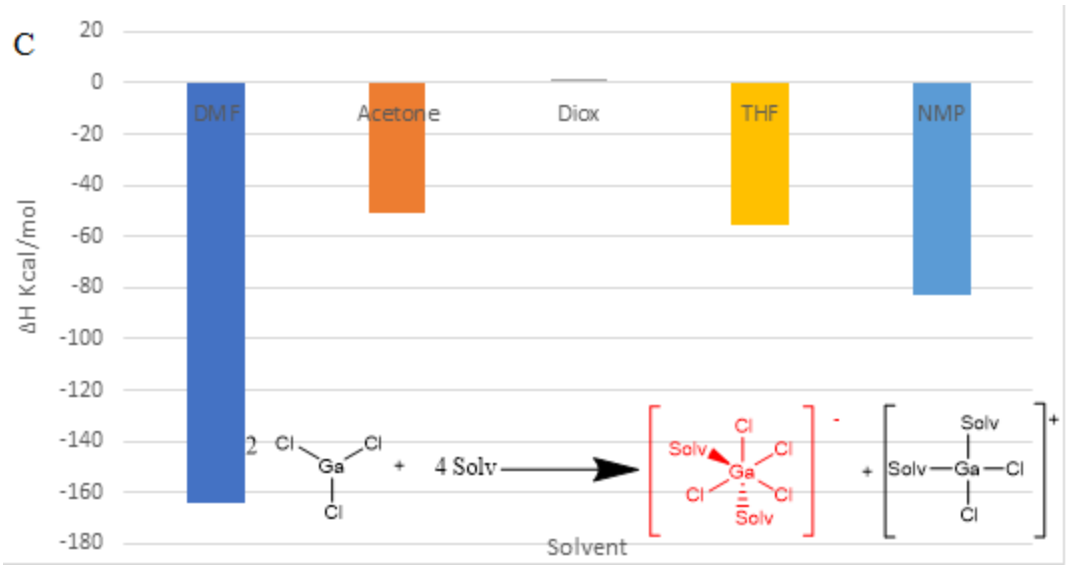

Figure 33: Ionization phases with increasing solvent from A, B to C.

The di-solvate anion with an octahedral structure, $[GaCl_4(solv)_2]^-$, is enthalpically most favored, bar graph C. Figure 33. Un-solvated tetrahedral $GaCl_4^-$, bar graph B above, is formed via an enthalpically favored reaction. Following the isolation of $GaCl_4^-$ and the different analyses done including attempts to reproduce it for MOF synthesis and outcomes involved, identifying the form of the ionized Ga-intermediate remains to be a challenge because of the inconsistencies seen in the characterization. They include its ability to synthesize a MOF with BTC but not with TDC attempts despite setting suitable synthesis conditions. Additionally, the $GaCl_4$TEA behaves differently upon solvation in organic solvents by forming double bands in DMF and single band in NMP and THF, hence a challenge assigning respective bands in *in situ* Raman solvation exercise. Table in Figure 34, outlines the enthalpy change as observed in ionization and solvation of $GaCl_3$.

Solvation/ ionization → products / Solvent ↓	1. $GaCl_3$(solv)	2. $GaCl_3$(2 Solv)	3. $GaCl_3$(3solv)	4. $GaCl_4^-$ + $[GaCl_2(solv)]^+$	4. $GaCl_4^-$ + $[GaCl_2(2solv)]^+$	5. $GaCl_4(solv)2$ + $[GaCl_2(2solv)]^+$
DMF	-60.0	-92.2	-122.3	-50.5	-113.1	-164.4
Acetone	-31.5	-34.4	-48.5	-16.6	-56.9	-51.2
Diox	-27.6	-32.0	–	-7.0	-31.1	1.8
THF	-33.4	-45.6	-57.8	-16.1	-58.9	-55.3
NMP	-40.0	-51.0	-40.3	-30.7	-76.4	-82.9

Figure 34: Enthalpy data for solvation and ionization of $GaCl_3$. Numbers are in units of Kcal/mol.

Solvation of $Ga(NO_3)_3$ on the other hand showed a similar trend where coordination with more solvent ligands was favored enthalpically, Figure 35 A and B. Enthalpy change doubled with the increase of solvent ligands to two. DMF showed the highest solubilization potential. However, the shortcomings of studying this salt in computer simulations was the inability to converge some of the bulky molecules. Additionally, the experimental analysis of $Ga(NO_3)_3$ presented a challenge in due to insolubility at room temperatures in the selected organic solvents and at Raman sustained temperatures.

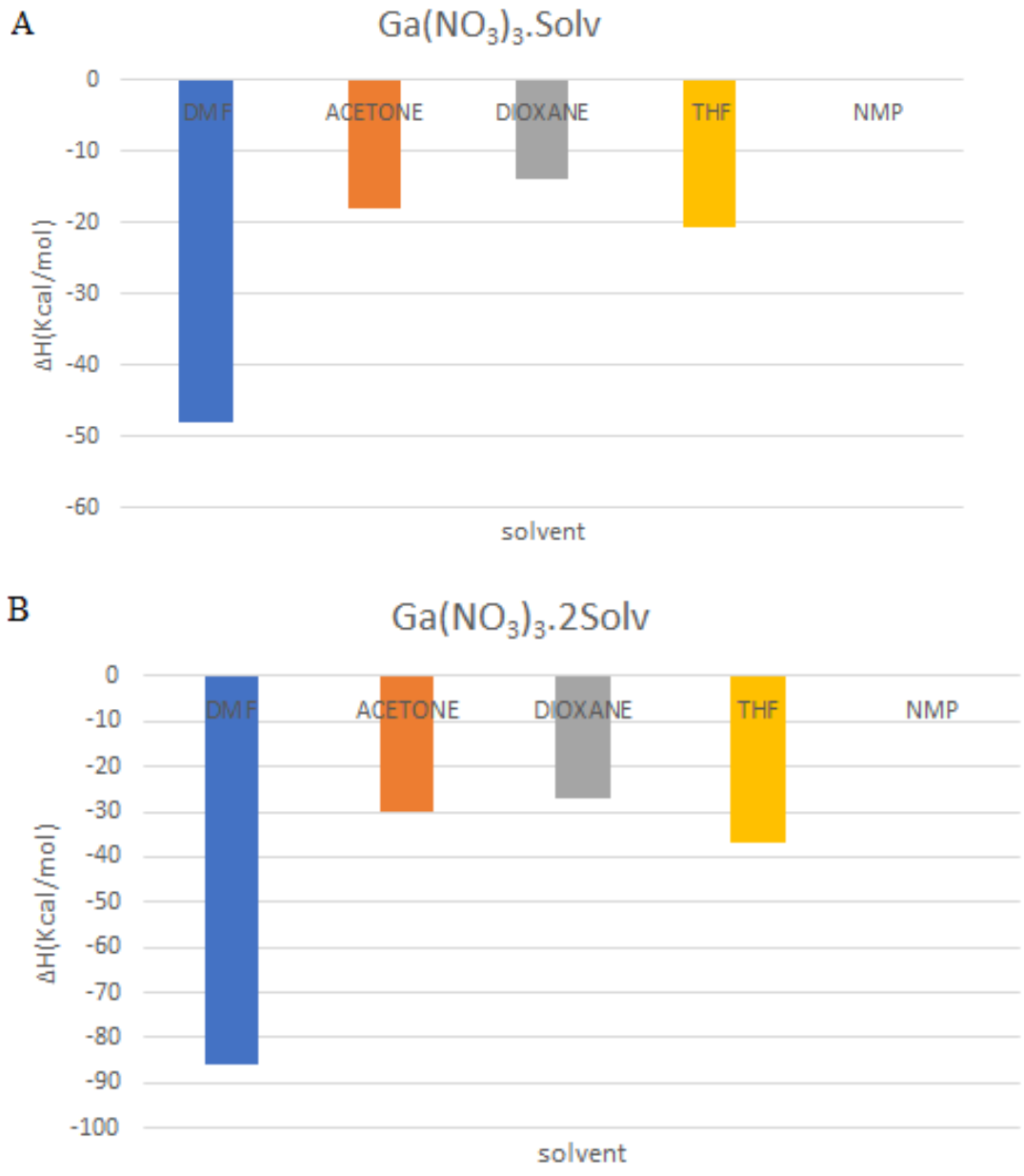

Figure 35: Enthalpy change in $Ga(NO_3)_3$ solvation.

3.3 *In situ* Raman for $GaCl_3$ in solution

A significant phase in the reaction for MOF synthesis translates into a high-intensity band on the contour graphs built from *in situ* Raman data when compared to other regions as described previously in the Ga-MOF synthesis examples. The Raman band at 345 cm^{-1} was also present in the solvation of $GaCl_4TEA$ but is yet to be assigned the form in which it presents.

From the simulation calculations, the most probable outcome from the dissolution of $GaCl_3$ is ionization. The resulting product $GaCl_4^-$ can be assigned the peaks/ Raman bands formed from *in situ* analysis as occurring in a solvated or unsolvated form observed consistently with the discussed experiments. Solvothermal MOF synthesis can take place in single solvents or in mixed solvent systems. Solvation analyses in (DMF, NMP, THF and dioxane) resulted in the Raman bands shown in the contour graphs below. Figure 36.

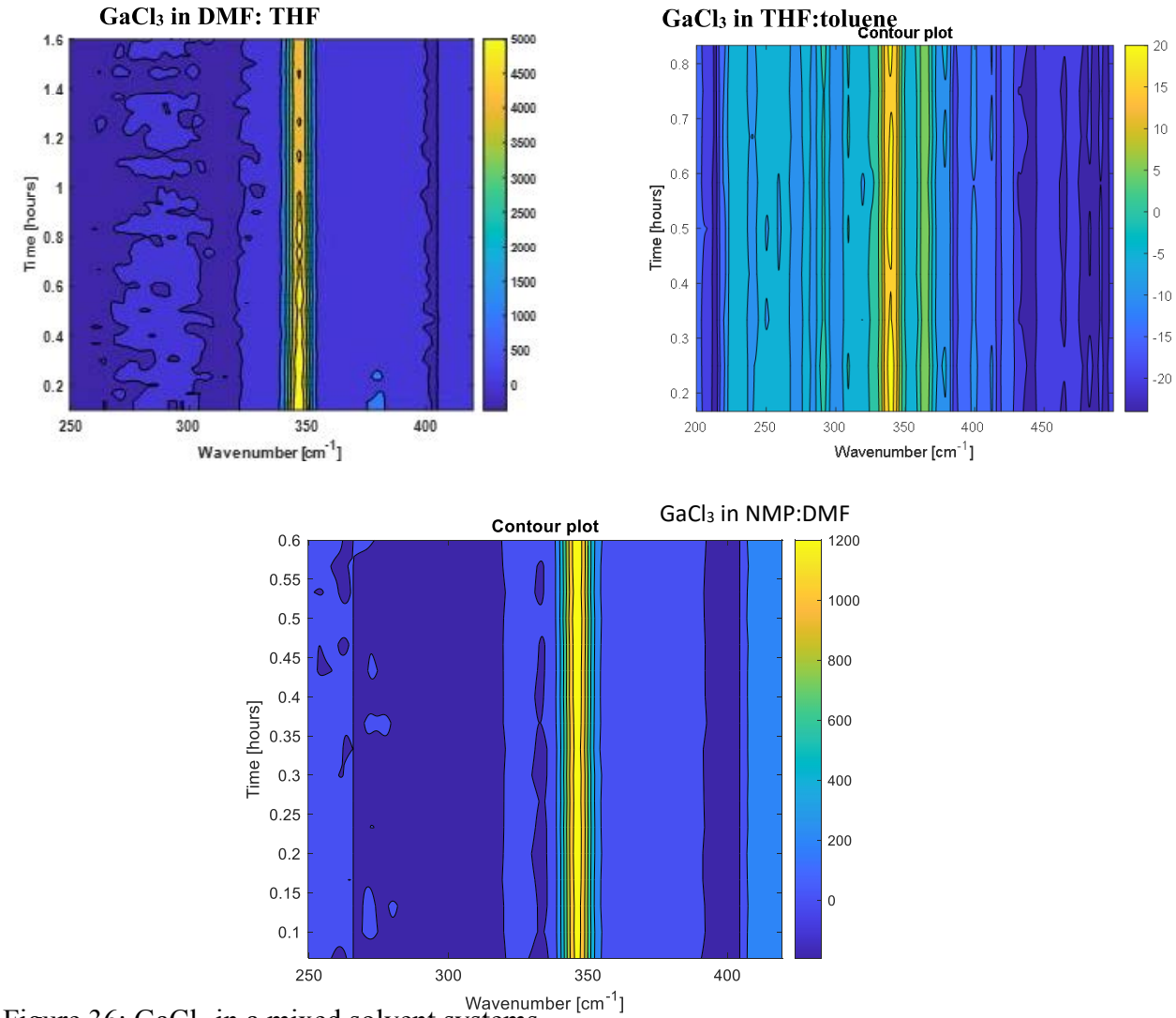

Figure 36: $GaCl_3$ in a mixed solvent systems.

$GaCl_3$ dossolved readily in mixed solvent system and the Raman analysis showed an intense band at the 345 cm^{-1}, as similarly observed in past experiments. This further confirmed the hypothesis of ionization preference of Ga^{3+} in solution to form the tetrachloride form in line with the DFT calculations and the matching peaks/ bands of $GaCl_4^-$ solvation.

In single solvent systems, solvation of $GaCl_3$, a single Raman band at 345 cm^{-1} was observed in DMF and NMP. Recall that, in previous solvation of $GaCl_4$TEA in DMF, two bands were observed in the contour graph at 345 cm^{-1} and 410 cm^{-1} whereas a single Raman band was formed in NMP. this means a possibility of different chemical phases, probably a $GaCl_3$ solvate and the unsolvated $GaCl_4^-$ occurring at the 345 cm^{-1} peak that we are not able to differentiate at this point.

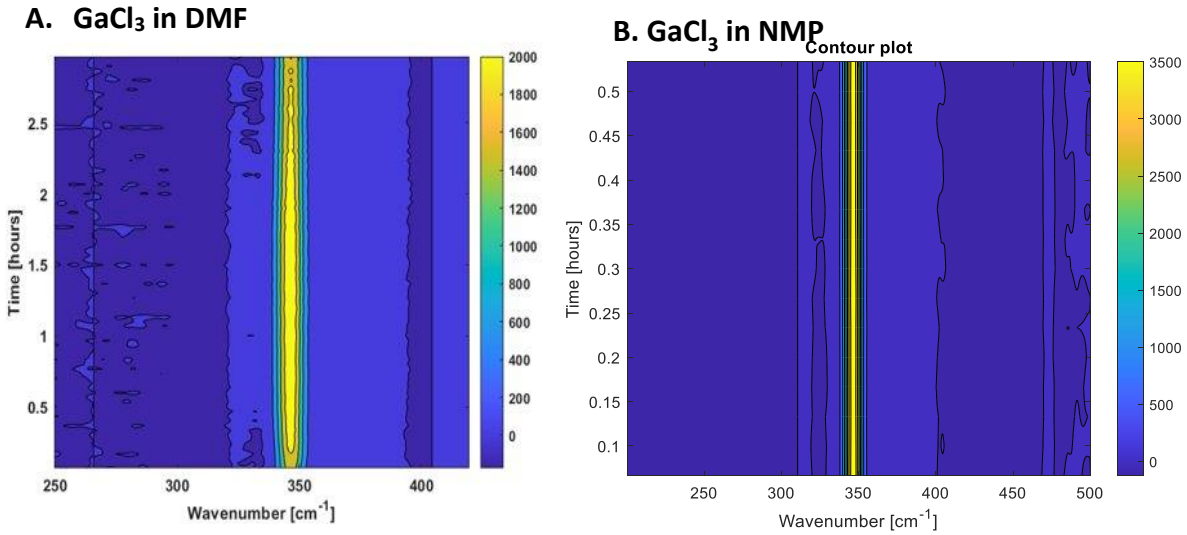

Figure 37: Contour graphs showing 345 cm-1 peak for $GaCl_3$ in **A.** DMF and **B.** NMP single solvent system.

On the other hand, solvation of $GaCl_3$ in dioxane and THF resulted in a Raman band at 365 cm^{-1}. Considering that, the salt completely goes into solution upon dissolving, called for further analysis to identify the possible compound formed.

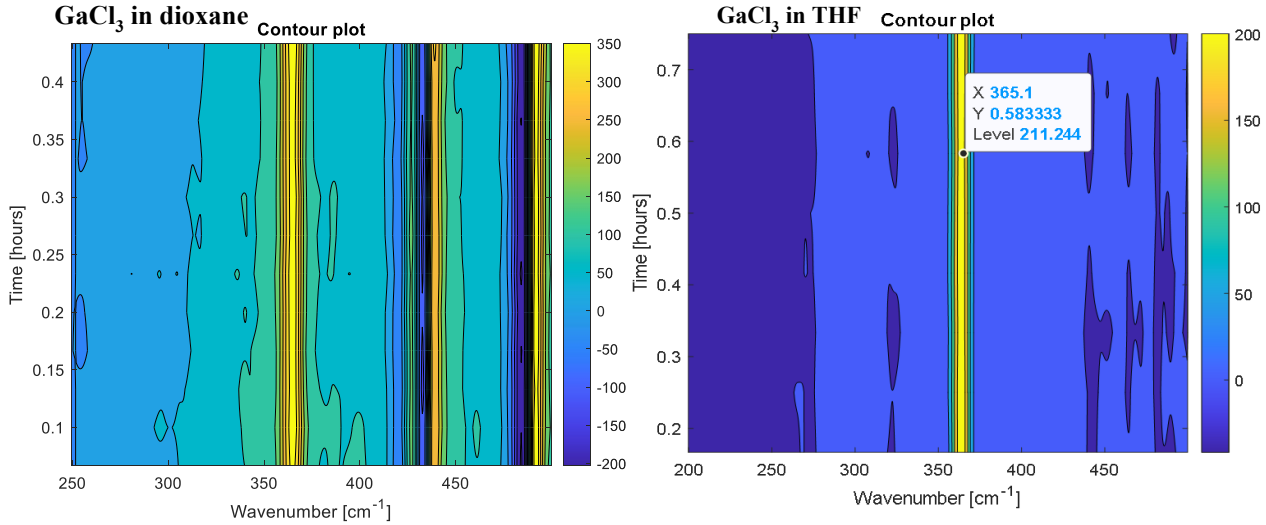

Figure 38: Contour graphs for Raman band at 365 cm^{-1}.

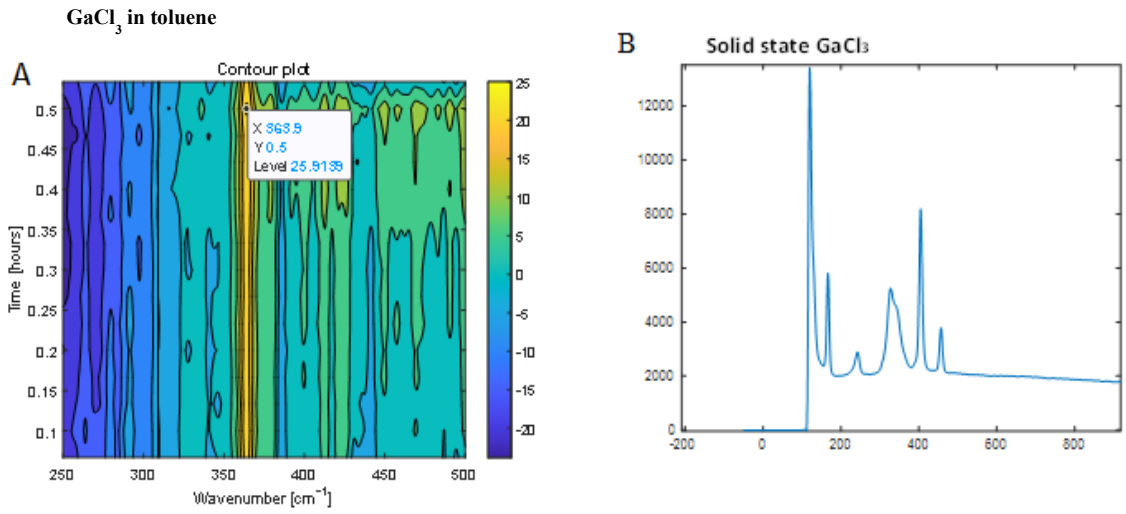

Figure 39: A. $GaCl_3$ in toluene and B. Solid-state Raman for $GaCl_3$.

$GaCl_3$ in dioxane, THF and toluene showed a peak at 365 cm^{-1}. Due to the non-coordinating chemical nature of toluene, the resulting bands are probable phase of $GaCl_3$ in solution. However, the solid-state Raman for $GaCl_3$ which exists commercially as a dimer, shows no peak at 365 cm^{-1} to match the phase represented in solution, hence we can assign it as unsolvated monomer $GaCl_3$ subject for further analysis.

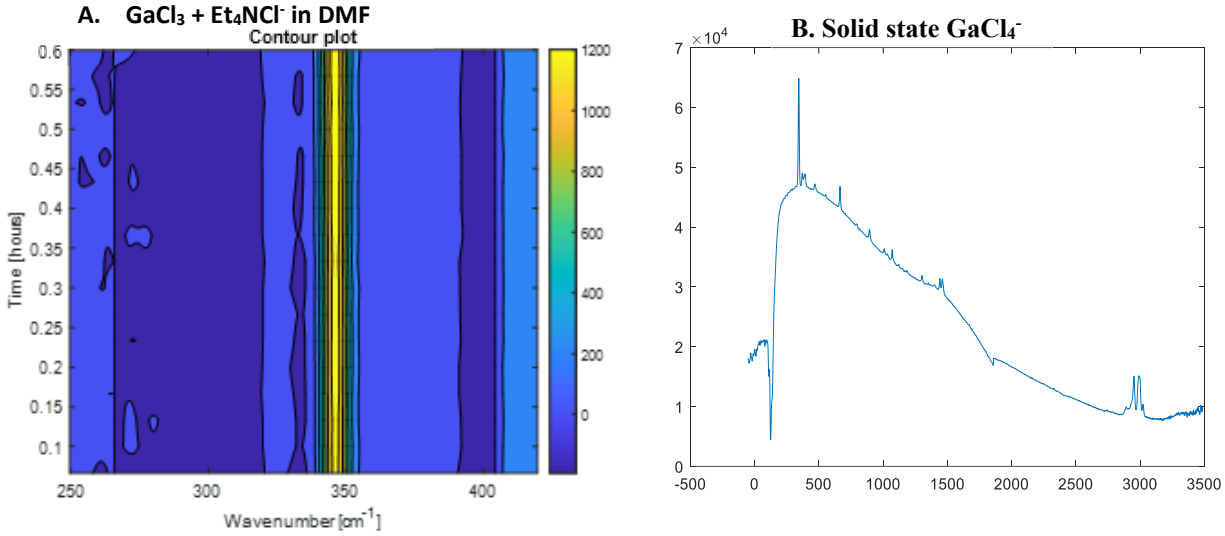

Figure 40:A. *in situ* and B. solid-state Raman analysis of $GaCl_3 + Et_4N^+Cl^-$

The registered initial transformations of Ga^{3+} in MOF reaction includes formation of disolvated or unsolvated $GaCl_4^-$. Monitoring this starting material with other additives like linker and modulator

generated the contour graphs below. In the presence of a TDC linker and suitable synthesis conditions, $GaCl_4^-$ doesn't form any MOF product and *in situ* Raman analysis of the reaction shows that the starting material is not consumed over time. On the other hand, $GaCl_4^-$ in the presence of BTC resulted in CAUMOF-11 and the *in situ* Raman indicated that $GaCl_4^-$ was consumed over time in the process as the intensity in the 345 cm^{-1} peak declines.

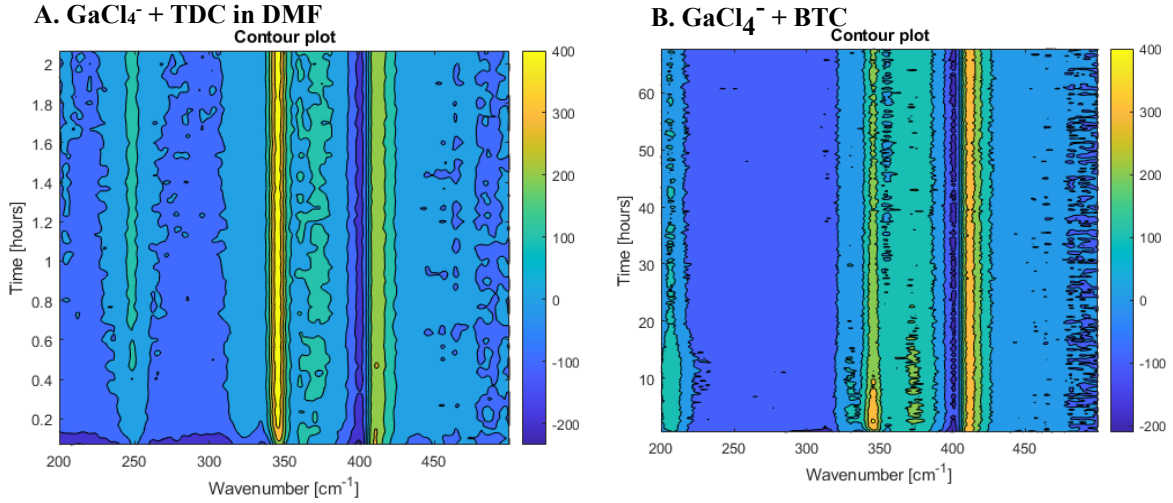

Figure 41: Contour plots for A) $GaCl_4^-$ + TDC in DMF, B) $GaCl_4^-$ + BTC in DMF

To get a clear clarity on the differences between role of $GaCl_3$ and $GaCl_4^-$ we designed experiments where the compounds were added to solvent one at a time. When $GaCl_3$ dissolved in THF is monitored for half an hour before addition of $GaCl_4$TEA, there are two peaks at 345 cm^{-1} and 365 cm^{-1} whose intensity is low. The initial peak intensity increases upon addition of the tetrachloride. This shows that the 345 cm^{-1} peak represents a form of $GaCl_3$ that we are yet to establish besides the unsolved $GaCl_4^-$. Figure 42.

On the other hand, a similar stepwise analysis in DMF gives three Raman bands at 345 cm^{-1}, 365 cm^{-1} and 410 cm^{-1}. The unsolved $GaCl_4^-$ band appears immediately in a contour graph at the start of the reaction. The Raman band representative of TEA also shows up at the start of the reaction and can be attributed to the decomposition of DMF. Figure 42.

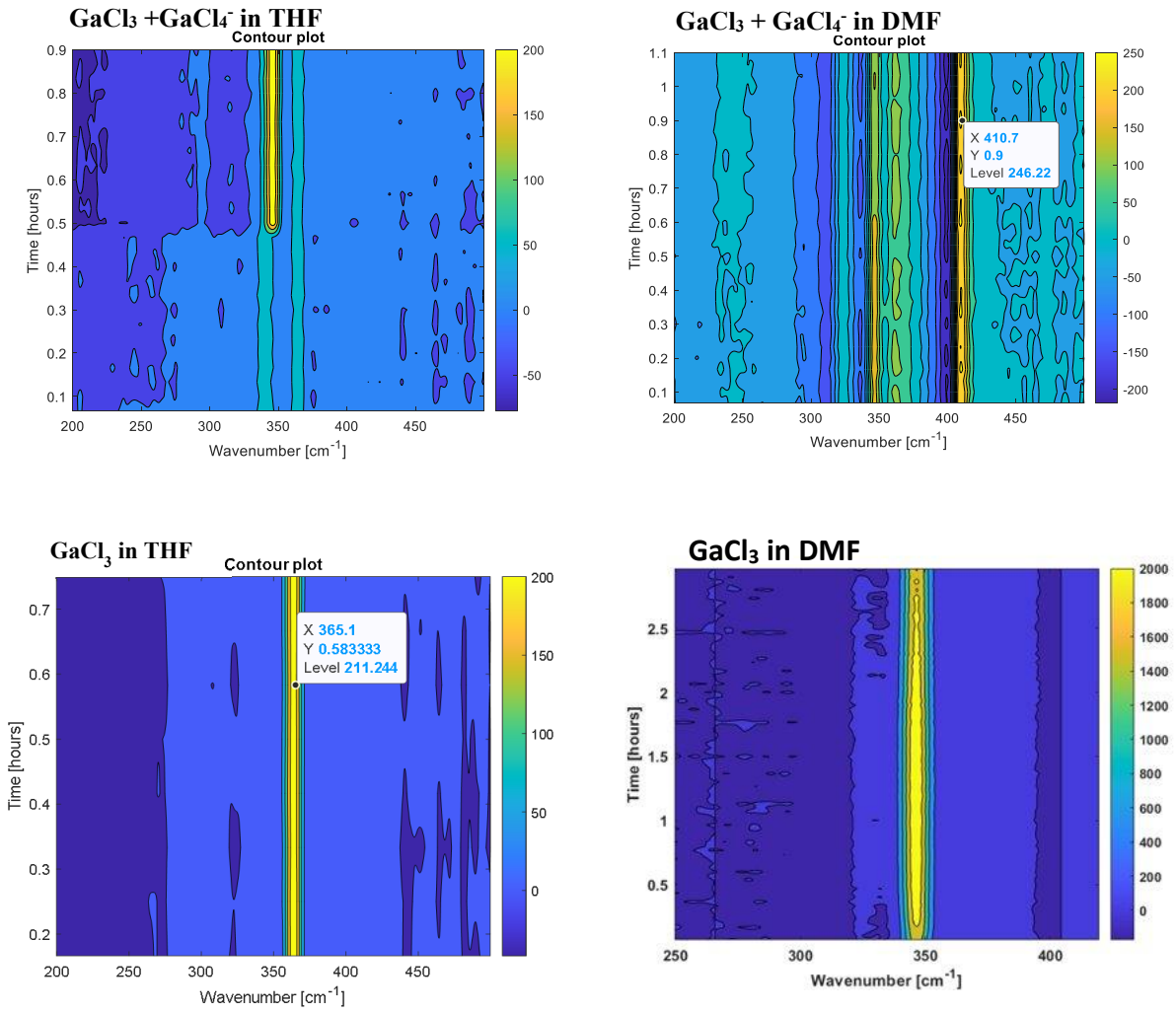

Figure 42: Raman bands at 345 cm^{-1} and 365 $cm^{-1}$with $GaCl_3$ but shows up upon addition of $GaCl_4^-$ in THF. The 345cm^{-1} peak shows up, upon dissolving $GaCl_3$ in DMF.

CHAPTER IV: CONCLUSION

Synthesis of new anionic Ga-MOFs are still a challenge despite having computational proof that thermodynamically, they should be able to form. Ideally, a node formed from the starting materials is a template out of which MOFs grow with differently coordinating ligands to yield variety of polymers. The possibility of this with Ga as the metal center is work in progress were there are still a number of aspects that needs to be studied further with Ga. Firstly, a node for anionic MOFs was arrived at after traversing several intermediates. Isolating the MOF intermediate $GaCl_4^-$ and evidently using it for MOF synthesis is also an affirmation that this is a step ahead in the understanding how Ga-MOFs form. If more of the intermediates can be isolated and characterized, there will be a realization of new anionic Ga-MOFs or a general understanding on the points of manipulation.

From solvation analyses, we were able to verify that $GaCl_3$ ionization is a feasible process and an important step in anionic CAUMOF-11 synthesis whereby transformation into $GaCl_4^-$ is necessary and its unsolvated form can result in the MOF with right synthesis conditions. However, we cannot overlook the inconsistencies in solvation characterization where *in silico* findings do not agree with experimental results hence need for further studies.

It is interesting that low polarity solvents can provide medium for synthesis of MOFs as in the case of CAUMOF-11 synthesis in toluene: dioxane. DMF has been the most preferred solvent for MOF synthesis since the many roles it plays in MOF synthesis including providing ions for reaction besides solubilization of starting materials. DMF behaves differently from the other solvents but still the other solvents have something to offer in MOF synthesis. If their role is understood, will provide alternative medium besides contributing to the library of information on MOF syntheses.

In situ Raman data brought into perspective the transformations taking place within a reaction. A combination of computational calculations, synthesis and spectroscopy played a huge role in identification, isolation and characterization of intermediates and products. In this case, $GaCl_4^-$ was predicted in the roadmap, feasibility of its formation was indicated by the DFT calculations, *in situ* Raman picked up its presence in reaction mixture and synthetic product was confirmed using solid-state Raman as well as PXRD. Essentially, the combination of both techniques build confidence on the outcomes by providing meaningful information about inputs, intermediates, reactions and end products.

References

(1) Tatebe, C. J.; Yusuf, S.; Bellas, M. K.; Zeller, M.; Arntsen, C.; Genna, D. T. On the Role of Dioxane in the Synthesis of In-Derived MOFs. *Cryst. Growth Des.* **2021**, *21* (12), 6840–6846. https://doi.org/10.1021/acs.cgd.1c00766.

(2) D'Alessandro, D. M. Exploiting Redox Activity in Metal–Organic Frameworks: Concepts, Trends and Perspectives. *Chem. Commun.* **2016**, *52* (58), 8957–8971. https://doi.org/10.1039/C6CC00805D.

(3) Thorarinsdottir, A. E.; Harris, T. D. Metal–Organic Framework Magnets. *Chem. Rev.* **2020**, *120* (16), 8716–8789. https://doi.org/10.1021/acs.chemrev.9b00666.

(4) Kreno, L. E.; Leong, K.; Farha, O. K.; Allendorf, M.; Van Duyne, R. P.; Hupp, J. T. Metal–Organic Framework Materials as Chemical Sensors. *Chem. Rev.* **2012**, *112* (2), 1105–1125. https://doi.org/10.1021/cr200324t.

(5) Lawson, H. D.; Walton, S. P.; Chan, C. Metal–Organic Frameworks for Drug Delivery: A Design Perspective. *ACS Appl. Mater. Interfaces* **2021**, *13* (6), 7004–7020. https://doi.org/10.1021/acsami.1c01089.

(6) Schilling, L.-H.; Reinsch, H.; Stock, N. Synthesis, Structure, and Selected Properties of Aluminum-, Gallium-, and Indium-Based Metal-Organic Frameworks. In *The Chemistry of Metal-Organic Frameworks: Synthesis, Characterization, and Applications*; Kaskel, S., Ed.; Wiley-VCH Verlag GmbH & Co. KGaA: Weinheim, Germany, 2016; pp 105–135. https://doi.org/10.1002/9783527693078.ch5.

(7) Liu, X.-Y.; Lo, W.-S.; Wu, C.; Williams, B. P.; Luo, L.; Li, Y.; Chou, L.-Y.; Lee, Y.; Tsung, C.-K. Tuning Metal–Organic Framework Nanocrystal Shape through Facet-Dependent Coordination. *Nano Lett.* **2020**, *20* (3), 1774–1780. https://doi.org/10.1021/acs.nanolett.9b04997.

(8) Karagiaridi, O.; Bury, W.; Sarjeant, A. A.; Hupp, J. T.; Farha, O. K. Synthesis and Characterization of Functionalized Metal-Organic Frameworks. *J. Vis. Exp.* **2014**, No. 91, 52094. https://doi.org/10.3791/52094.

(9) Moghadam, P. Z.; Li, A.; Wiggin, S. B.; Tao, A.; Maloney, A. G. P.; Wood, P. A.; Ward, S. C.; Fairen-Jimenez, D. Development of a Cambridge Structural Database Subset: A Collection of Metal–Organic Frameworks for Past, Present, and Future. *Chem. Mater.* **2017**, *29* (7), 2618–2625. https://doi.org/10.1021/acs.chemmater.7b00441.

(10) Lu, W.; Wei, Z.; Gu, Z.-Y.; Liu, T.-F.; Park, J.; Park, J.; Tian, J.; Zhang, M.; Zhang, Q.; Gentle III, T.; Bosch, M.; Zhou, H.-C. Tuning the Structure and Function of Metal–Organic Frameworks via Linker Design. *Chem Soc Rev* **2014**, *43* (16), 5561–5593. https://doi.org/10.1039/C4CS00003J.

(11) Zhang, H.; Ding, Z.-J.; Luo, Y.-H.; Geng, W.-Y.; Wang, Z.-X.; Zhang, D.-E. Assembly of a Rod Indium–Organic Framework with Fluorescence Properties for Selective Sensing of Cu^{2+}, Fe^{3+} and Nitroaromatics in Water. *CrystEngComm* **2022**, *24* (3), 667–673. https://doi.org/10.1039/D1CE01312B.

(12) Mihaly, J. J.; Zeller, M.; Genna, D. T. Ion-Directed Synthesis of Indium-Derived 2,5-Thiophenedicarboxylate Metal–Organic Frameworks: Tuning Framework Dimensionality. *Cryst. Growth Des.* **2016**, *16* (3), 1550–1558. https://doi.org/10.1021/acs.cgd.5b01680.

(13) Rabe, T.; Grape, E. S.; Rohr, H.; Reinsch, H.; Wöhlbrandt, S.; Lieb, A.; Inge, A. K.; Stock, N. Isoreticular Chemistry of Group 13 Metal–Organic Framework Compounds Based on V-Shaped Linker Molecules: Exceptions to the Rule? *Inorg. Chem.* **2021**, *60* (12), 8861–8869. https://doi.org/10.1021/acs.inorgchem.1c00767.

(14) Yan, J.; Jiang, S.; Ji, S.; Shi, D.; Cheng, H. Metal-Organic Framework MIL-53(Al): Synthesis, Catalytic Performance for the Friedel-Crafts Acylation, and Reaction Mechanism. *Sci. China Chem.* **2015**, *58* (10), 1544–1552. https://doi.org/10.1007/s11426-015-5359-0.
(15) So, P. B.; Tang, P.-H.; Liao, B.-S.; Sathishkumar, N.; Chen, H.-T.; Lin, C.-H. Sustainable Scale-up Synthesis of MIL-68(Al) Using IPA as Solvent for Acetic Acid Capture. *Microporous Mesoporous Mater.* **2021**, *316*, 110943. https://doi.org/10.1016/j.micromeso.2021.110943.
(16) Wu, T.; Prasetya, N.; Li, K. Recent Advances in Aluminium-Based Metal-Organic Frameworks (MOF) and Its Membrane Applications. *J. Membr. Sci.* **2020**, *615*, 118493. https://doi.org/10.1016/j.memsci.2020.118493.
(17) Fischer, S.; Roeser, J.; Lin, T. C.; DeBlock, R. H.; Lau, J.; Dunn, B. S.; Hoffmann, F.; Fröba, M.; Thomas, A.; Tolbert, S. H. A Metal–Organic Framework with Tetrahedral Aluminate Sites as a Single-Ion Li^+ Solid Electrolyte. *Angew. Chem. Int. Ed.* **2018**, *57* (51), 16683–16687. https://doi.org/10.1002/anie.201808885.
(18) Sun, H.-X.; Wang, H.-N.; Fu, Y.-M.; Meng, X.; He, Y.-O.; Yang, R.-G.; Zhou, Z.; Su, Z.-M. A Multifunctional Anionic Metal–Organic Framework for High Proton Conductivity and Photoreduction of CO_2 Induced by Cation Exchange. *Dalton Trans.* **2022**, *51* (12), 4798–4805. https://doi.org/10.1039/D2DT00089J.
(19) Mihaly, J. J.; Zeller, M.; Genna, D. T. Ion-Directed Synthesis of Indium-Derived 2,5-Thiophenedicarboxylate Metal–Organic Frameworks: Tuning Framework Dimensionality. *Cryst. Growth Des.* **2016**, *16* (3), 1550–1558. https://doi.org/10.1021/acs.cgd.5b01680.
(20) Volkringer, C.; Meddouri, M.; Loiseau, T.; Guillou, N.; Marrot, J.; Férey, G.; Haouas, M.; Taulelle, F.; Audebrand, N.; Latroche, M. The Kagomé Topology of the Gallium and Indium Metal-Organic Framework Types with a MIL-68 Structure: Synthesis, XRD, Solid-State NMR Characterizations, and Hydrogen Adsorption. *Inorg. Chem.* **2008**, *47* (24), 11892–11901. https://doi.org/10.1021/ic801624v.
(21) Volkringer, C.; Meddouri, M.; Loiseau, T.; Guillou, N.; Marrot, J.; Férey, G.; Haouas, M.; Taulelle, F.; Audebrand, N.; Latroche, M. The Kagomé Topology of the Gallium and Indium Metal-Organic Framework Types with a MIL-68 Structure: Synthesis, XRD, Solid-State NMR Characterizations, and Hydrogen Adsorption. *Inorg. Chem.* **2008**, *47* (24), 11892–11901. https://doi.org/10.1021/ic801624v.
(22) Kareem, H. M.; Abd Alrubaye, R. Th. Synthesis and Characterization of Metal Organic Frameworks for Gas Storage. *IOP Conf. Ser. Mater. Sci. Eng.* **2019**, *518* (6), 062013. https://doi.org/10.1088/1757-899X/518/6/062013.
(23) Akhbari, K.; Morsali, A. Effect of the Guest Solvent Molecules on Preparation of Different Morphologies of ZnO Nanomaterials from the [Zn_2 (1,4-Bdc)$_2$ (Dabco)] Metal-Organic Framework. *J. Coord. Chem.* **2011**, *64* (20), 3521–3530. https://doi.org/10.1080/00958972.2011.623778.
(24) Yakovenko, A. A.; Wei, Z.; Wriedt, M.; Li, J.-R.; Halder, G. J.; Zhou, H.-C. Study of Guest Molecules in Metal–Organic Frameworks by Powder X-Ray Diffraction: Analysis of Difference Envelope Density. *Cryst. Growth Des.* **2014**, *14* (11), 5397–5407. https://doi.org/10.1021/cg500525g.
(25) Burrows, A. D.; Cassar, K.; Friend, R. M. W.; Mahon, M. F.; Rigby, S. P.; Warren, J. E. Solvent Hydrolysis and Templating Effects in the Synthesis of Metal–Organic Frameworks. *CrystEngComm* **2005**, *7* (89), 548. https://doi.org/10.1039/b509460g.

(26) Brozek, C. K.; Michaelis, V. K.; Ong, T.-C.; Bellarosa, L.; López, N.; Griffin, R. G.; Dincă, M. Dynamic DMF Binding in MOF-5 Enables the Formation of Metastable Cobalt-Substituted MOF-5 Analogues. *ACS Cent. Sci.* **2015**, *1* (5), 252–260. https://doi.org/10.1021/acscentsci.5b00247.
(27) Wu, Y.; Moorhouse, S. J.; O'Hare, D. Time-Resolved *in Situ* Diffraction Reveals a Solid-State Rearrangement During Solvothermal MOF Synthesis. *Chem. Mater.* **2015**, *27* (21), 7236–7239. https://doi.org/10.1021/acs.chemmater.5b03085.
(28) Yuan, W.; O'Connor, J.; James*, S. L. Mechanochemical Synthesis of Homo- and Hetero-Rare-Earth(Iii) Metal–Organic Frameworks by Ball Milling. *CrystEngComm* **2010**, *12* (11), 3515. https://doi.org/10.1039/c0ce00216j.
(29) Pichon, A.; Lazuen-Garay, A.; James, S. L. Solvent-Free Synthesis of a Microporous Metal–Organic Framework. *CrystEngComm* **2006**, *8* (3), 211. https://doi.org/10.1039/b513750k.
(30) Shoaee, M.; Anderson, M. W.; Attfield, M. P. Crystal Growth of the Nanoporous Metal-Organic Framework HKUST-1 Revealed by In Situ Atomic Force Microscopy. *Angew. Chem. Int. Ed.* **2008**, *47* (44), 8525–8528. https://doi.org/10.1002/anie.200803460.
(31) Xu, H.; Sommer, S.; Broge, N. L. N.; Gao, J.; Iversen, B. B. The Chemistry of Nucleation: In Situ Pair Distribution Function Analysis of Secondary Building Units During UiO-66 MOF Formation. *Chem. – Eur. J.* **2019**, *25* (8), 2051–2058. https://doi.org/10.1002/chem.201805024.
(32) Goesten, M. G.; de Lange, M. F.; Olivos-Suarez, A. I.; Bavykina, A. V.; Serra-Crespo, P.; Krywka, C.; Bickelhaupt, F. M.; Kapteijn, F.; Gascon, J. Evidence for a Chemical Clock in Oscillatory Formation of UiO-66. *Nat. Commun.* **2016**, *7* (1), 11832. https://doi.org/10.1038/ncomms11832.
(33) Millange, F.; Medina, M. I.; Guillou, N.; Férey, G.; Golden, K. M.; Walton, R. I. Time-Resolved In Situ Diffraction Study of the Solvothermal Crystallization of Some Prototypical Metal-Organic Frameworks. *Angew. Chem.* **2010**, *122* (4), 775–778. https://doi.org/10.1002/ange.200905627.
(34) El Osta, R.; Feyand, M.; Stock, N.; Millange, F.; Walton, R. I. Crystallisation Kinetics of Metal Organic Frameworks From *in Situ* Time-Resolved X-Ray Diffraction. *Powder Diffr.* **2013**, *28* (S2), S256–S275. https://doi.org/10.1017/S0885715613000997.
(35) Embrechts, H.; Kriesten, M.; Hoffmann, K.; Peukert, W.; Hartmann, M.; Distaso, M. Elucidation of the Formation Mechanism of Metal–Organic Frameworks via in-Situ Raman and FTIR Spectroscopy under Solvothermal Conditions. *J. Phys. Chem. C* **2018**, *122* (23), 12267–12278. https://doi.org/10.1021/acs.jpcc.8b02484.
(36) Embrechts, H.; Hartmann, M.; Peukert, W.; Distaso, M. In Situ Monitoring of Particle Formation with Spectroscopic and Analytical Techniques Under Solvothermal Conditions. *Chem. Eng. Technol.* **2020**, *43* (5), 879–886. https://doi.org/10.1002/ceat.201900520.
(37) Stavitski, E.; Goesten, M.; Juan-Alcañiz, J.; Martinez-Joaristi, A.; Serra-Crespo, P.; Petukhov, A. V.; Gascon, J.; Kapteijn, F. Kinetic Control of Metal-Organic Framework Crystallization Investigated by Time-Resolved In Situ X-Ray Scattering. *Angew. Chem. Int. Ed.* **2011**, *50* (41), 9624–9628. https://doi.org/10.1002/anie.201101757.
(38) Cravillon, J.; Schröder, C. A.; Nayuk, R.; Gummel, J.; Huber, K.; Wiebcke, M. Fast Nucleation and Growth of ZIF-8 Nanocrystals Monitored by Time-Resolved In Situ Small-Angle and Wide-Angle X-Ray Scattering. *Angew. Chem.* **2011**, *123* (35), 8217–8221. https://doi.org/10.1002/ange.201102071.

(39) Hausdorf, S.; Wagler, J.; Moβig, R.; Mertens, F. O. R. L. Proton and Water Activity-Controlled Structure Formation in Zinc Carboxylate-Based Metal Organic Frameworks. *J. Phys. Chem. A* **2008**, *112* (33), 7567–7576. https://doi.org/10.1021/jp7110633.
(40) Embrechts, H.; Kriesten, M.; Ermer, M.; Peukert, W.; Hartmann, M.; Distaso, M. Role of Prenucleation Building Units in Determining Metal–Organic Framework MIL-53(Al) Morphology. *Cryst. Growth Des.* **2020**, *20* (6), 3641–3649. https://doi.org/10.1021/acs.cgd.9b01384.
(41) Cantu, D. C.; McGrail, B. P.; Glezakou, V.-A. Formation Mechanism of the Secondary Building Unit in a Chromium Terephthalate Metal–Organic Framework. *Chem. Mater.* **2014**, *26* (22), 6401–6409. https://doi.org/10.1021/cm5027859.
(42) Lee, T.; Chang, Y. H.; Lee, H. L. Crystallization Process Development of Metal–Organic Frameworks by Linking Secondary Building Units, Lattice Nucleation and Luminescence: Insight into Reproducibility. *CrystEngComm* **2017**, *19* (3), 426–441. https://doi.org/10.1039/C6CE02246D.
(43) *The Chemistry of Metal-Organic Frameworks: Synthesis, Characterization, and Applications: Synthesis, Characterization, and Applications*; Kaskel, S., Ed.; Wiley-VCH Verlag GmbH & Co. KGaA: Weinheim, Germany, 2016. https://doi.org/10.1002/9783527693078.
(44) Lee, D. W.; Jo, V.; Ok, K. M. Solvothermal Synthesis, Crystal Structure, and Second-Order Nonlinear Optical Properties of a New Noncentrosymmetric Gallium-Organic Framework Material, [N(C3H7)4]3Ga3[C6H3(CO2)3]4. *J. Solid State Chem.* **2012**, *194*, 369–374. https://doi.org/10.1016/j.jssc.2012.06.005.
(45) Schmulbach, C. D.; Ahmed, I. Y. Spectral and Conductance Study of Gallium Trihalides and Their Complexes in Acetonitrile. *Inorg. Chem.* **1971**, *10* (9), 1902–1907. https://doi.org/10.1021/ic50103a013.
(46) Sun, Y.-X.; Zhang, S.-T.; Ren, Z.-L.; Dong, X.-Y.; Wang, L. Synthesis, Characterization, and Crystal Structure of a New Supramolecular Cd ^{II} Complex With Halogen-Substituted Salen-Type Bisoxime. *Synth. React. Inorg. Met.-Org. Nano-Met. Chem.* **2013**, *43* (8), 995–1000. https://doi.org/10.1080/15533174.2012.753614.